UNIVERSITY OF LEEDS

This is a repository copy of *Revisiting the black shale depositional enigma: Transport processes and contrasting sediment sources in a heterolithic basin fill – Bowland Basin, England*.

White Rose Research Online URL for this paper:
https://eprints.whiterose.ac.uk/228731/

Version: Accepted Version

Article:
Li, S., Wignall, P.B. orcid.org/0000-0003-0074-9129, Peakall, J. orcid.org/0000-0003-3382-4578 et al. (2 more authors) (Cover date: June 2025) Revisiting the black shale depositional enigma: Transport processes and contrasting sediment sources in a heterolithic basin fill – Bowland Basin, England. Sedimentology, 72 (4). pp. 1132-1165. ISSN 0037-0746

https://doi.org/10.1111/sed.13271

This is an author produced version of an article published in Sedimentology made available under the terms of the Creative Commons Attribution License (CC-BY), which permits unrestricted use, distribution and reproduction in any medium, provided the original work is properly cited.

Reuse
This article is distributed under the terms of the Creative Commons Attribution (CC BY) licence. This licence allows you to distribute, remix, tweak, and build upon the work, even commercially, as long as you credit the authors for the original work. More information and the full terms of the licence here: https://creativecommons.org/licenses/

Takedown
If you consider content in White Rose Research Online to be in breach of UK law, please notify us by emailing eprints@whiterose.ac.uk including the URL of the record and the reason for the withdrawal request.

White Rose university consortium
Universities of Leeds, Sheffield & York

eprints@whiterose.ac.uk
https://eprints.whiterose.ac.uk/

Revisiting the black shale depositional enigma: transport processes and contrasting sediment sources in a heterolithic basin fill – Bowland Basin, England

SEN LI[1,3], PAUL B. WIGNALL[3], JEFF PEAKALL[3], JINGWEI CUI[2,3], YADONG SUN[1]

1. State Key Laboratory of Biogeology and Environmental Geology, China University of Geosciences, Wuhan 430074, China

2. PetroChina Research Institute of Petroleum Exploration & Development, Beijing, 100083, China

3. School of Earth and Environment, University of Leeds, Leeds LS2 9JT, UK

Short Title – Black shale depositional enigma

ABSTRACT

Factors that control the accumulation of organic-rich shales are keenly debated and include basin redox variations, sediment provenance and diverse depositional processes. The relative importance of hemipelagic settling versus sediment gravity flows has been especially contentious in recent years. This study examines the Bowland Shale, a thick succession of organic-rich mudrock with subsidiary facies, from the late Mississippian Bowland Basin of northern England that records a broad range of depositional processes. Interbedded amongst the mudrocks are several elongate, calciturbidite fans *ca* 10 km in length, sourced from a small carbonate platform to the south-east of the basin, whilst a turbidite body of siliciclastic sand entered the basin from the east. An intrabasinal high in the north-west of the basin deflected the progradation of the turbidite sandstones and was likely also responsible for the reflection of the carbonate-carrying sediment gravity flows generating combined flow structures in the calciturbidite fans. Abundant, fine calcareous detritus was also sourced from the south-east, forming an apron of calcareous mudstone delivered by low-strength debris flows. Interbedded amongst these diverse facies types, the Bowland Shale primarily consists of hemipelagic, organic-rich shale with a fabric consisting of compacted clay lenses (0.05 – 0.4 mm in width), hemipelagic components (including larval shells of bivalves, goniatites and syngenetic framboids) and organic filaments (marine snow). The lenses are interpreted to be faecal pellets formed above the redoxcline before settling to the seabed. An alternative idea, that has gained much traction in mudrock studies, is that the clay lenses are transported intraclasts and that black shales are substantially the product of deposition from traction currents sourced from adjacent basin margins. This idea is problematic because it fails to address why basinal shales have a euxinic geochemical signature rather than recording the well-oxygenated conditions of the purported source area.

Key words: Black shale, calciturbidite fans, clay lens fabric, faecal pellets, hemipelagic

INTRODUCTION

The infill of marine sedimentary basins is a product of their interaction with the surrounding shelf seas, sediment supply routes, tectonism and prevailing climate, and it can be especially complex when both clastic and carbonate sediment source areas are active. The degree of water column stratification is a further variable, controlled by climate and water balance in the basin, resulting in deposition beneath anoxic bottom waters (Demaison & Moore, 1980; Algeo *et al*., 2007). Basinal black shale deposition often onlaps onto surrounding shallow-water carbonate platforms, a relationship that can record transgressive drowning (Schlager, 1981), the collapse of the basin margin on transition to a sag phase (e.g. Pickard *et al*., 1994) and/or the shut-down of the carbonate factory caused by multiple potential factors such as ocean acidification, climate cooling and expansion of eutrophic basinal waters into shallower settings (e.g. Hallock & Schlager, 1986; Krencker *et al*., 2014; Petrash *et al*., 2016; Reijmer, 2021; Andrieu *et al*., 2022; Li *et al.,* 2022). Distinguishing between these alternatives is challenging with no general model predicting black shale–carbonate platform interactions. Recent advances in the understanding of basinal processes have added further complexity with many mudrocks now widely regarded to be predominantly accumulations of intraclasts transported by sediment gravity flows from shallower settings (e.g. Schieber *et al*., 2010; Könitzer *et al.,* 2014; Emmings *et al.,* 2020a; Li *et al.,* 2021) rather than the 'traditional' view that they primarily record hemipelagic deposition (e.g. Wignall, 1994; Gorsline *et al*., 1996). The new interpretations require shallow-water mudrock 'staging areas' to be present before the mud reaches its final destination within the basin.

Many of these inter-related factors were likely important in the deposition of the Bowland Shale: a major black shale formation developed in the Bowland Basin of northern England during the late Mississippian. This basin records a prolonged history of organic-rich, shale-dominated deposition, spanning *ca* 10 Myr, in a series of deep-water settings surrounded by platform carbonates. The resultant mudrocks are an important hydrocarbon resource for shale gas exploration in the region (Gross *et al*., 2015; Clarke *et al*., 2018; Hennissen & Gent, 2019; de Jonge-Anderson & Underhill, 2020). The Bowland Shale is referred to as a hemipelagic mudstone by some authors (Waters *et al*., 2009, 2020; de Jonge-Anderson & Underhill, 2020), but the past decade has seen a succession of studies of this, and other similar black shale formations, that propose deposition was from debris flows, low concentration turbidity currents and hybrid flows that transported mud rip-up clasts from upper slope and shelf settings (e.g. Könitzer *et al*., 2014; Gross *et al*., 2015; Newport *et al*., 2018, 2020; Emmings *et al*., 2020a; Li *et al*., 2021; Peng, 2021; Wei & Swennen, 2022). The Bowland Shale also contains coarser-grained units, including the Pendleside Sandstone and several calcarenite horizons (see below), that undoubtedly record sediment transport from shallower water areas, but to ascribe a similar origin to the mudrocks challenges the assumption that basinal shales provide a reliable record of basinal geochemistry. A fundamental question is if the shale consists of clasts supposedly derived from upslope oxic shelf settings, then what redox signal do they record?

This study aims to examine the controls on sedimentation in the Bowland Basin. Specifically, the following questions are addressed:

1) What was the relative importance of siliciclastic versus carbonate detritus?

2) How did the clastic sediments reach the basin?

3) Were eustatic changes important?

4) What depositional processes controlled fine-grained deposition?

Ultimately, this study provides an insight into the complexities of black shale deposition in a basin flanked by shallow-water carbonate platforms increasingly influenced by encroaching clastic systems. This analysis has broader implications for understanding the relative importance of the potentially diverse controls on the deposition of basinal mudrocks and their veracity as a repository for redox conditions within basins.

REGIONAL HISTORY

Bowland Shale deposition began in the late Asbian Stage during a phase of active tectonism that transformed ramp carbonate systems (of the Pendleside Limestone Formation) into a series of laterally-linked, fault-bounded basins flanked by carbonate platforms and shelf seas (Gawthorpe, 1986; Kirby *et al*., 2000; Fraser & Gawthorpe, 1990; Fig. 1). The Bowland Basin was the western-most of the onshore basins and is the focus of this study (Fig. 1B). Following active rifting around the Asbian/Brigantian boundary, the basins transitioned into a sag phase by the end Brigantian (Gawthorpe, 1986; Leeder, 1988; Waters *et al.,* 2017a; Hennissen & Gent, 2019), although local active tectonism was intermittently developed as late as the Pendleian Stage (Dunham & Wilson, 1985; Kirby *et al*., 2000; Kane *et al*., 2010). Carbonate slope deposits of the Pendleside Limestone Formation were replaced by the mudrocks of the Bowland Shale, which developed diachronously from the late Asbian to Brigantian. The lower part of the Bowland Shale also includes limestone (e.g. Park Style Limestone Member and Ravensholme Limestone Member) and sandstone units (e.g. Pendleside Sandstone Member) (Fig. 1C). Deposition was oxygen-restricted with ferruginous or weakly euxinic waters initially developed. Strongly euxinic conditions were widespread by the Pendleian (Li *et al*., 2024, 2025). Better ventilation in the basin only occurred shortly before mudrock deposition was terminated by the influx of the Pendle Grit Formation, a major turbidite sandbody (Emmings *et al*., 2020b).

Variations in basinal accommodation are controlled by subsidence and sediment supply and, for much of the depositional history considered here, the former outpaced the latter because at no point were shallow-water conditions developed. Water depths during Bowland Shale deposition are considered to have been at least several hundred metres (Black, 1940; Kirby *et al*., 2000; Emmings *et al*., 2020a). Even after the influx of major sandbodies, such as the 450 m thick Pendle Grit, basinal conditions persisted. Nonetheless, base-level variations driven by glacioeustasy are also thought to have influenced deposition within the basin (Pharaoh *et al*., 2020).

The Bowland Shale subcrop is extensive over large areas of central northern England, where the formation is of economic interest as a hydrocarbon source (e.g. Clark *et al*., 2018; de Jonge-Anderson & Underhill, 2020). Deposition occurred in several linked basins but only the Bowland Basin of central Lancashire has experienced later basin inversion (Pharaoh *et al*., 2020). Consequently, this area provides the best-available exposures of the Bowland Shale which have been the focus of much recent study. The Bowland Basin trends north-east/south-west, is around 25 km in width and at least 40 km in length, although it may have extended for up to twice this distance to the south-west in subcrop (Kirby *et al.,* 2000; Waters *et al*., 2009; Figs 1B and 2). The northern margin was bounded by the Askrigg Block, a structurally stable area that saw shallow-water carbonates accumulating concurrently with the Bowland Shales. The transition between basin and platform occurred in the Craven Fault Belt, an area bounded by the North and South Craven faults that diverged to the south-east forming a structurally complex area over 15 km wide to the north-east of the Bowland Basin (Fig. 2). These faults were active during Bowland Shale deposition, strongly controlling thickness variations (see below) and local uplift and erosion in hanging wall sites (Hudson, 1930; Waters *et al.,* 2017a). The transition from active rifting to a thermal sag phase in the early Brigantian did little to affect the northern extent of Bowland Shale, which was marked by the line of the North Craven Fault throughout its depositional history.

During the Asbian and early Brigantian, fringing reefs (carbonate mudmounds) of the Cracoe Limestone Formation developed along the narrow belt between Mid Craven and North Craven faults and separated the carbonate platform of the Askrigg Block to the north from the Bowland Basin to the south (Kirby *et al*., 2000; Waters *et al*., 2017a,b). The subsequent demise of the mudmounds, perhaps due to uplift and emergence, was followed by onlap of the Bowland Shale, which sits atop these former topographic highs. Contemporaneously, on the Askrigg Block carbonate platform, the mudmound demise coincides with a change from limestones to the more heterolithic facies of the Yoredale Group, although carbonates continued to dominate deposition until the Pendleian when siltstone and minor sandstones became more prevalent (Arthurton *et al*., 1988). The lateral transition between the Bowland Shale and the Yoredale Group is remarkably abrupt, occurring over a distance of a few hundred metres (Black, 1950; Li *et al*., 2024). Minor conglomeratic debris flows are suggested to have transported Askrigg Block carbonates into the Bowland Basin (Brandon *et al*., 1998; Clarke *et al*., 2018) and Emmings *et al*. (2020a) consider that the mudrock facies of the Bowland Shale were sourced from deltas on the Askrigg Block.

The south-east margin of the Bowland Basin was also delineated by a series of faults that are today associated with the Pendle monocline structure (Kirby *et al*., 2000; Clarke *et al*., 2018; Pharaoh *et al*., 2020). To the south-east of this structure lay the north-east/south-west trending Central Lancashire High. This carbonate platform was not connected with the Askrigg Block carbonate platform because Bowland Shale deposition occupies the Craven Fault Belt region in the intervening area (Fig. 2). The Central Lancashire High is unexposed. However, borehole evidence indicates that (unlike the Askrigg Block), it foundered during the

Pendleian and was onlapped by the Bowland Shale (Kirby *et al*., 2000). The north-west margin of the Bowland Basin is marked by the Bowland High, which separates it from the Lancaster Fells Basin where Bowland Shale also accumulated (Kirby *et al*., 2000). Black shale deposition is continuous between these two basins, indicating that the Bowland High was an intrabasinal high but not a markedly shallower water area (Arthurton *et al*., 1988). Around 5 km to the south-east of the Bowland High and parallel with it, the Slaidburn Anticline formed another intrabasinal high with a remarkably condensed Bowland Shale record developed upon it (Fig. 2; Earp *et al.,* 1961). These north-east/south-west trending anticlinal structures were probably generated by contemporaneous, dextral, strike-slip movements of the Craven Fault Belt (Arthurton, 1984; Kirby *et al*., 2000; Clarke *et al*., 2018). To the south-west, the Bowland Basin broadens and passes into the Irish Sea Basin, where the Bowland Shale has sourced the gas fields of the region (Fig. 1; Clarke *et al*., 2018).

METHODS AND APPROACH

Fieldwork investigations (sedimentary logging and sample collection) have been undertaken at 16 locations, primarily in the Bowland Basin and Craven Reef Belt but also on the basin margin and Askrigg Block (Table 1). High-resolution correlation in the Bowland Shale is accomplished using a goniatite fauna that is detailed in literature that dates back a century and in the memoirs of the British Geological Survey. This literature has also been used, together with our field measurements, to construct isopach maps and correlation panels for the Bowland Shale and its non-shale members. These utilise both thicknesses measured at outcrop and the estimated thicknesses from the Geological Survey's maps. Contouring was undertaken by hand because data density is insufficient for more advanced quantitative techniques such as kriging.

Facies analysis was undertaken based on field and petrographic observations. A total of 182 samples were thin-sectioned and petrographically examined using a polarising microscope. Facies were named based on their composition and grain size. In addition, 96 samples were polished, carbon-coated and analysed on a TESCAN VEGA3 Scanning Electron Microscope (SEM; Tescan, Brno, Czech Republic) in backscatter mode to investigate the size and morphology of pyrite grains. The components of the calcarenite lithologies were quantified by point counting to assess evolution on the adjacent carbonate platform source area. A total of 42 calcarenite thin sections were examined from different locations. Usually more than 10 photomicrographs were used to identify at least 100 bioclasts for statistical analysis and lithology description. The proportion of certain type of bioclasts is obtained by its abundance over total abundance of bioclasts in the sample. The three most abundant bioclast types are shown in detail (see below) while others are grouped into 'other bioclasts' for clear display. The sandstones of the Pendleside Sandstone Member are thoroughly described elsewhere (Clarke *et al*., 2018) and are not a focus of this study.

RESULTS

Regional development of Bowland Shales

The Asbian–Brigantian portion of the Bowland Shale shows substantial thickness changes ranging from *ca* 50 m to >300 m within the Bowland Basin and Craven Fault Belt area to the north (Fig. 3). The variation is strongly controlled by faulting with an elongate depocentre developed in the hanging wall to the south of the South Craven Fault whilst a more localized depocentre occurs to the south of the Mid Craven Fault (Fig. 3). Peak thickness of the lower part of the Bowland Shale is however developed in the centre of the Bowland Basin (Fig. 3). This is principally caused by the development of the Pendleside Sandstone

Member (see below). Rapid lateral thickness variations in the mudrocks of the lower Bowland Shale are also seen at the zonal and subzonal scale (e.g. the P_{1a} shales and early P_2 shales show rapid lateral thickness change; Fig. 4), suggesting active faulting within the basin. The thinnest lower Bowland Shale deposits are adjacent to the Slaidburn Anticline, although they are still stratigraphically complete on this intrabasinal high (e.g. Smelthwaite Farm section in Fig. 4, Section A). Following the demise of the fringing belt of carbonate mudmounds in the earliest Brigantian (Waters *et al*., 2017a), Bowland Shale deposition expanded into the Craven reef belt region, as seen in the Fell Lane section, where black shales are interbedded with carbonate boulder beds and coarse crinoidal calcarenites (Fig. 5).

The Bowland Shale Formation includes the Pendleside Sandstone Member, a substantial turbidite sandstone body (cf. Clarke *et al*., 2018) developed around the P_1 – P_2 boundary (Fig. 6). Several shale breaks occur within the Pendleside Sandstone [recorded by Earp *et al*. (1961) and Clarke *et al.* (2018)], and it is possible that more detailed investigation could resolve this unit into individual, stacked sandbodies. The Pendleside Sandstone isopachs show peak thickness (>200 m) in the centre of the Bowland Basin and an abrupt termination of its western development against the Slaidburn Anticline structure (Fig. 7), where it thins from 200 m to 0 m in a distance of only *ca* 2 km (Earp *et al*., 1961, p.81). This suggests that the Slaidburn Anticline was a topographic barrier to turbidite progradation, whilst the expansion of the Pendleside Sandstone's area to the south and (to a lesser extent) to the north of this structure indicates the high was only *ca* 10 km in length. This allowed the sands to continue to expand around the margins (Fig. 7).

To the east of its development, the area of Pendleside Sandstone rapidly contracts, but a narrow outcrop of contemporaneous sandstone occurs to the east of Skipton (Fig. 7). This sandstone body is *ca* 50 m thick and has been locally named the Nettleber Sandstone

(Hudson & Mitchell, 1937). It probably passes eastward into the Harlow Hill Sandstone, which occurs within the Bowland Shale of the adjacent Harrogate Basin (Fig. 1). A borehole in this basin showed 49 m of Harlow Hill Sandstone developed below black shales with P_{2a} goniatites (Cooper & Burgess, 1993). This elongate sand body (cf. Fig. 7) was likely a feeder channel for the Pendleside Sandstone.

The lower part of the Bowland Shale also contains frequent beds of limestone, either as isolated, decimetric to metre-scale tabular sheets or more substantial, mappable limestone-dominated intervals (Fig. 8). These latter strata have been named the Park Style Limestone Member and the Ravensholme Limestone Member. Isopach maps show that the limestone bodies are of much more restricted extent than the Pendleside Sandstone. Based on their outcrop distribution, both have a broadly north-south alignment and have widths (of *ca* 5 km) that were less than their length, giving them a linear outline (Fig. 8). Their occurrences, restricted to the southern part of the Bowland Basin, suggest that they were sourced from the carbonate platform on the Central Lancashire High to the south-east, whilst suggestions that some calciturbidites were sourced from the Askrigg Block (e.g. Clark *et al*., 2018) is not supported. At outcrop, the limestone lithologies consist of both calcarenite and calcisiltite lithologies and are described below. Both the Park Style and Ravensholme limestones consist of amalgamated beds of carbonate in their thickest, axial development, but they pass into interbedded mudrock and limestone off axis (e.g. Tory Log Clough section, Fig. 4). Geochemical analysis of the shales interbedded with the carbonates indicates weak anoxia during deposition (Li *et al*., 2024). This contrasts with the euxinic signature from contemporaneous basinal shales (Li *et al*., 2024), perhaps indicating that the limestone carbonate fans were elevated above the more reducing, deepest waters of the basin.

Thickness trends of the Pendleian-portion of the Bowland Shale show more subdued variations, especially within the Bowland Basin, with the Slaidburn Anticline no longer affecting deposition (Fig. 9). This may be partly because there are no major sandstone or limestone units within the formation (Figs 6 and 9). However, the Hind Sandstone, a thin, turbidite sandstone body in the Lancaster Fells Basin to the north-west, may have just reached the margins of the Bowland Basin, but its distribution and lateral extent are limited (Aitkenhead *et al*., 1992). To the east of Skipton, limited exposures of a crinoidal limestone indicate the presence of a carbonate fan of a comparable thickness (*ca* 50 m) to those lower in the Bowland Shale (Fig. 8). This is the E_{1a} age Berwick Limestone (Hudson & Mitchell, 1937), and its rapid pinching out, to both the east and west suggests that the outcrop is a cross-section of a north–south orientated fan like those seen lower in the Bowland Shale.

Maximum thicknesses of the Pendleian-aged Bowland Shale occur in hanging wall settings adjacent to the South and Mid Craven faults (Figs 6 and 9), indicating tectonic-controlled depocentres. The interval between the Brigantian and Pendleian saw reactivation and uplift of the South Craven Fault resulting in a locally-developed unconformity within the Bowland Shale (Dixon & Hudson, 1931; Arthurton *et al*., 1988). Thus, at the School Share location P_2 shales are truncated and onlapped by E_{1b} shales (Fig. 4). Higher in this section, irregular bodies composed of angular limestone boulders (up to 3 m in dimension) occur within the shale. These are likely sourced from Brigantian limestones immediately to the north (Hudson, 1930; Dixon & Hudson, 1931). Carbonate boulder beds, typically only a metre or so thick, also occur locally in the Bowland Basin (Fig. 8), and have been suggested to be debris-flow deposits sourced from the Askrigg Block (Aitkenhead *et al*., 1992).

In its northern-most development, the Bowland Shale passes laterally over a short distance into the more heterolithic strata of the Yoredale Group (Fig. 6). No exposure displays the transition, but field mapping around Grassington shows that it occurs over a distance of only *ca* 200 m (Black, 1950). This boundary closely approximates with the line of the North Craven Fault although the most northerly Bowland Shale outcrops occur to the north of this structure. It is unlikely that a steep palaeoslope, between deep-water black shales and shallow-water heterolithics, occurred in the 200 m wide transition zone (no evidence of slope failure is seen) suggesting that the basin margin black shales were deposited in a similar water depth to the Yoredale strata which are generally regarded as shallow-marine facies. However, elsewhere large boulders of limestone are found in the Bowland Shale (described below), suggesting submarine fault scarps of appreciable height were developed at least locally at the basin margin.

Carbonate Lithofacies (CLF)

Coarse calcirudites: CLF 1

Coarse calcirudites are developed within the Bowland Shale close to the northern boundary faults (School Share and Fell Lane locations, Figs 4 and 5). They have limited lateral extent and at School Share an extensive exposure shows they form an irregular breccia 10 m thick and 15 m wide embedded in shales. The breccia is clast supported and bedding in the individual clasts is at high angles to the bedding in the Bowland Shale. The limestone boulders range from centimetre up to metre-sized and have been sourced from nearby, *in situ* carbonates at the margin of the Askrigg Black (Hudson, 1930; Dixon & Hudson, 1931). At Fell Lane, CLF 1 occurs in erosive-based beds with large, flat pebbles of reworked Bowland Shale, a few centimetres thick and up to 50 cm in width, developed in the upper part of beds (Fig. 10A and B). The matrix of this facies is diverse, and is composed of micritic mudstone and skeletal components (including large crinoidal columnals, brachiopods, bryozoans and rugose corals) and patches of coarse, sparry cement (Fig. 11A and B).

Calcarenite (peloid–foram–crinoid pack-grainstone): CLF 2

Packstone and grainstone beds are a common component of the limestone bodies in the Bowland Shale (Fig. 5). Beds are sharp based, sometimes with groove marks, and have a thickness which is typically 10 to 30 cm. Internally they can be massive to weakly graded, planar laminated, or sometimes show internal scours (Fig. 10C to E). At the condensed Smelthwaite Farm location (Fig. 4, Section A), CLF 2 grainstones infill broad, erosive hollows ranging from 5 to 30 cm deep and up to 2 m wide. Other beds often display hummock-like bedforms, typically a few centimetres in height and a metre across (Fig. 10D), but the larger examples reach 20 cm thickness and 2 m in width (Fig. 10E). Internal laminae record simple aggradational growth (Fig. 10F).

The CLF 2 beds are well sorted with an average grain size of 0.4 mm, although in some beds they can be coarser (Fig. 11C to F). In some horizons the peloids deviate from a normally well-rounded appearance and can be somewhat angular, which may indicate that they are tiny intraclasts or bioclasts rather than peloids *sensu stricto*. Peloids (*sensu lato*) and foraminifera are the major components of CLF 2 but there is also a range of bioclasts including brachiopods, calcispheres, crinoids and bryozoans. Well-developed micritic coatings are common, especially on crinoid grains (Fig. 11D).

The clast content of CLF 2 beds varies throughout the history of the Bowland Basin. The ramp carbonates of the preceding Pendleside Limestone Formation are primarily composed of peloids and microspheres but there is an upward transition to crinoid-dominated grainstones in the Bowland Shale (Fig. 12). Greater diversity is seen in the Fell Lane section, developed immediately adjacent to a carbonate mudmound (*ca* 1 km distant) where fragments of corals and bryozoans as well as crinoids dominate bioclasts. The Berwick Limestone was not sampled during this study, but Hudson & Mitchell (1937) reported it to be composed of crinoid detritus like other Bowland Shale carbonates. The exception to this crinoid-dominated detritus are the thin CLF 2 beds, developed on the condensed intrabasinal high at Smelthwaite Farm, where peloids and small foraminifera are seen (Fig. 11).

Calcisiltites: CLF 3

Beds of calcisiltite are common in the lower (Asbian–Brigantian) Bowland Shale where they occur as sharp-based, tabular beds a few centimetres thick and occasionally as decimetre-thick beds displaying swale-like cross lamination (e.g. in the lowermost Park Style Limestone outcrop at Dobson’s Brook, Fig. 4, Section A). Sediments are well-sorted, but can vary between beds in the range 0.02 mm to 0.05 mm (Fig. 13A and B). Occasionally coarser beds occur (e.g. in the latest Brigantian at Swardean Clough, Fig. 4, Section B) where the grain size reaches *ca* 0.1 mm indicating a gradation into CLF 2. Sponge spicules and small calcispheres are present but most grains are typically angular and of indeterminate origin; possibly finely comminuted shell material.

Laminated microspar: CLF 4

Limestone beds displaying swale-like cross-stratification and isolated hummock-like structures, 10 to 15 cm thick, are seen in Bowland Shale at Dinckley Hall (Fig. 4, Section B and Fig. 10C). In thin section the facies show fine lamination with wavy bedding consisting of alternations of micrite and fine microspar (Fig. 13C). Based on the similarity of their sedimentary structures, it is possible that the Dinckley Hall beds were originally CLF 2 beds that have undergone both recrystallization and micritization, but curiously no bioclasts remain. Laminated microspar is also seen in the Bowland Shale at the Smelthwaite Farm and Fell Lane locations where the fabric is dominated by laths of calcite 0.2 mm by 0.05 mm in size, with their long axis developed orthogonal to bedding, that sometimes show a slightly radiating or fan-like arrangement (Fig. 13D). Vestiges of clay lamination occur between the crystalline layers.

Bioclastic wackestone–mudstone: CLF 5

This is a rare facies in the lowest beds of the Bowland Shale, although it is more common in the underlying Pendleside Limestone. It is composed of dark micrite that sometimes shows aggrading neomorphism to fine microspar, together with bioclasts including small crinoid columnals, sponge spicules and ostracods (Fig.13E). In some examples, the bioclasts are predominantly calcispheres and small, thin-shelled bivalves (Fig. 13F). CLF 5 beds are homogenous, with bioclasts scattered throughout, and range in thickness from 20 to 50 cm.

Clastic Sandstone Lithofacies (CSF)

Fine to coarse grained sandstone: CSF 1

Tabular beds of sandstone ranging from a few centimetres up to one metre thick are developed in the lower part of the Bowland Shale where they form the Pendleside Sandstone Member (see above). In the Tory Log Clough section, stacked beds of CSF 1 occur at the base of the P_2 zones, but isolated sandstone beds of CSF 1 (and CSF 2 – see below) also occur up to 16 m below the base of this level in the P_{1d} subzone (Fig. 5). Here the thickest bed reaches 1.5 m and shows an internal erosion surface overlain by CSF 1 sandstone with low angle cross-beds. Thin sandstone beds are also seen in the upper Bowland Shale, appearing *ca* 20 m below the base of the coarse sandstones of the Pendle Grit Formation (Fig. 4), where frondescent marks (*sensu* Dżułyński & Walton, 1965) are seen on their base.

The CSF 1 sandstones are mainly composed of grains of both monocrystalline and polycrystalline quartz and feldspar that show considerable variation in their degree of rounding and sorting (Fig. 14A and B). The Pendleside Sandstone beds at Tory Log Clough show considerable inter-grain suturing and good sorting (grain size is around 0.1 – 0.2 mm; Fig. 14A). In contrast, the sandstones in the uppermost Bowland Shale at Dinckley Hall are poorly sorted (grain size varies from 0.1 – 2.0 mm) with the largest grains being well-rounded, whilst the angularity increases with decreasing grain size (Fig. 14B).

Fine-grained sandstone with bioclasts: CSF 2

This heterolithic lithofacies consists of decimetric beds that co-occur with CSF 1 beds below the Pendleside Sandstone at TLC in the P_{1d} subzone. The clastic content is the same as for CSF 1 but with the addition of bioclasts that constitute about 25% of the grains. These include crinoid columnals, foraminifera, and abraded fragments of brachiopods and bryozoans (Fig. 14C and D). The grain-size variation is comparable to that in the interbedded CSF 1 beds, with an average of 0.2 mm for both sandy grains and bioclasts.

Mudrock Lithofacies

Homogenous mudstone: MLF 1

Homogenous mudstones, often with indistinct bioturbation structures, are common in the uppermost Pendleside Limestone and the basal Bowland Shale, where they are restricted to beds of Asbian age (Fig. 15). MLF 1 beds are typically a few tens of centimetres thick. Besides their clay and minor carbonate content, they contain a low amount of organic filaments, pyrite and rare, silt-size calcareous and quartz grains. Fossils, including thin-shelled brachiopods, are rare (Fig. 16A).

MLF 2: Calcareous-argillaceous, silty mudstone

Calcareous-argillaceous, silty mudstone beds are common in the Bowland Shale up to the mid-Brigantian, with the proportion of silt-grade material varying considerably (Fig. 15). At outcrop, the facies can be blocky or weakly fissile. Beds range from decimetres to metres in thickness and are usually massive but can show diffuse lamination defined by alternations of calcareous-rich and clay-rich laminae. The clay grade material is dispersed throughout MLF 2 or it can occur as lenses similar to those in MLF 4 described below. The non-clay component is dominated by angular carbonate grains with a range of shapes, averaging 0.04 mm in size but with considerable variation (Fig. 16B, C and D), that are distributed throughout the fabric. These are too small to attribute to specific bioclast types, but they may be the highly fragmented detritus of the larger bioclasts that are occasionally present. These include crinoid columnals (ranging up to 2 mm in diameter, but typically <0.5 mm), thin-shelled bivalves and calcispheres. Pyrite framboids and quartz silt grains are also present, with the latter occasionally reaching up to 10% abundance.

Laminated, calcareous, silty mudstone: MLF 3

The MLF 3 facies occurs sporadically throughout the Bowland Shale and is a hard, platy, shale at outcrop. It is most common in the sections from the south-west of the Bowland Basin, which lie adjacent to the Central Lancashire High (Fig. 2). Laminations consist of alternations, on a 0.5 to 2.0 mm scale, between calcareous and silty mudstone layers. The latter are identical to the MLF 2 sediments (although they can be notably organic-rich) and contain a similar range of clasts. The calcareous layers are sharp-based and compositionally dominated by indeterminate, angular carbonate grains, minor quartz silt grains, lenses of micrite and occasionally peloids (Fig. 16E and F). The thicker laminae are sometimes erosive based and develop scours infilled with calcisilt lenses, but other laminae have diffuse boundaries.

Lenticular, organic-rich mudstone: MLF 4

Dark grey to black shales of MLF 4 occur throughout the Bowland Shale but are especially dominant in the upper (Pendleian-aged) Bowland Shale (Fig. 15). In thin sections, these are seen to consist of organic-rich mudstone with flattened clay lens structures that taper to a point. The clay-dominated lenses show a great size variation within individual layers, ranging from 0.05 mm to 0.4 mm in length and <0.06 mm in thickness and are embedded in a matrix of clay, organic matter, pyrite framboids and fine silt grains with occasional phosphatic nodules (Fig. 17A to F). Examination under SEM shows that there is no difference in mineral composition between clay lenses and the clay in the matrix (Fig. 17E). Occasionally lamina ranging from 1 to 5 mm thick occur in MLF 4 and consist of homogenous, organic matter-rich clay (Fig. 17C). Bioclasts, derived from the pelagic realm, are common in MLF 4 and include goniatite protoconchs, bivalve larval shells (prodissoconchs) (Fig. 17A), spar-filled calcispheres and chert-filled radiolarian tests (Fig. 17 and F). Unlike the bioclasts in other Bowland Shale facies, shells are consistently well preserved in MLF 4. Even the ultra-thin shells of prodissoconchs are rarely fragmented.

DISCUSSION

Carbonate depositional processes and platform resilience

The clast-supported, coarse calcirudites of CLF 1 occur adjacent to the faults of the Craven Fault Belt and are likely to have been shed from steep slopes generated during the active faulting phases. The large (metre-scale) angular clasts embedded in mudrock suggest rock fall/avalanche accumulations (Fig. 18). Additionally, minor conglomeratic debrites have been reported from around the Bowland (intrabasinal) High (Fig. 8), which are thought to have been sourced from the Askrigg Block (Brandon *et al*., 1998). The grooves at the base of CLF 2 beds record the passage of debris flows, where the matrix strength of the flow held a tool rigidly in place whilst dragging it across the substrate, thus forming the structures (Peakall *et al*., 2020; Baas *et al*., 2021b; McGowan *et al*., 2024).

The majority of carbonate beds in the Bowland Basin are well-sorted calcarenites or calcisiltites (CLF 2 and CLF 3) that occur as sharp-based, tabular beds that were likely deposited from waning turbidity currents (Fig. 18A). Most beds are massive or planar laminated, suggesting T_A and T_B divisions, but hummock-like and swale-like structures are seen in the south-west of the Basin, especially in the Park Styles Limestone (Figs 10D and 18A). The simple aggradational nature of these forms, the lack of internal cross-cutting relationships, and the continuity of laminae, suggest combined flow deposition (Tinterri, 2011; Hofstra *et al.,* 2018; Privat *et al*., 2021, 2024; Keavney *et al*., 2025) possibly due to the interaction between source turbidity currents and currents reflected from the Slaidburn Anticline. This structure was <5 km to the north-east of the Park Styles Limestone and clearly impeded the progress of the Pendleside Sandstone (cf. Fig. 8), suggesting that it was an intrabasinal high. Thus, carbonate-laden sediment gravity flows heading north-northwest from the Central Lancashire High could have reflected off this structure. These swale-like and hummock-like forms are unrelated to true swaley cross-stratification and hummocky cross-stratification (SCS and HCS), associated with storms in shallower waters which show internal cross-cutting relationships, and thickening and thinning of laminae (e.g. Harms *et al*., 1975; Jelby *et al*., 2020) not seen in the Bowland Shale examples. A few beds of CLF 2 are also found in the condensed Smelthwaite Farm section developed on the Slaidburn Anticline, an intrabasinal high where up to 2 m wide scours on one surface indicate occasional powerful flows on this structure.

The paucity of micrite in MLF 2 and MLF 3 could reflect efficient hydrodynamic sorting during turbulent flow, but there are no down-dip micrites known from the basin. More probably, it reflects a micrite-poor sediment source. The extensive carbonate platforms on the Askrigg Block were postulated to have sourced the Bowland Shale carbonates (Clarke *et al*., 2018). However, the restriction of the main carbonate bodies to the south-east of the basin suggests that they were being shed from the smaller Central Lancashire High (Fig. 8). The well-rounded bioclasts and abundance of calcisilt suggest prolonged agitation and winnowing on this platform with much abrasion and attrition of carbonate clasts together with a long-term shift from peloid to crinoid-dominated carbonate production (Fig. 12). The elongate nature of the principal carbonate bodies suggests that sediment was point sourced from the margin of the Central Lancashire High (Fig. 8). The authors can only speculate why this would be the case, but it might reflect a margin with a discontinuous fringe of reef mounds restricting sediment shedding to embayments between the reefs.

The failure of the Askrigg Block to supply carbonate detritus to the Bowland Basin is somewhat enigmatic. It has been suggested that the marginal reef belt developed along the Mid Craven Fault provided a barrier to carbonate shedding (Kirby *et al*., 2000; Waters *et al*., 2017a), but reef formation ceased in the earliest Brigantian and the mounds were onlapped by the Bowland Shale (Fig. 6). By the Pendleian, black shales had extended a short distance on to the Askrigg Block (Fig. 9) where they passed laterally into the shallow-water Yoredale

Group over a short distance. Therefore, after the Asbian, there was no topographic barrier between the Askrigg Block platform carbonates and the Bowland Basin to the south. A more likely reason for the lack of sediment transport from the Askrigg Block may come from the thickness trend of the Yoredale Group. The Group thickens northward from the footwall of the North Craven Fault (Wilson, 1960; Waters & Lowe, 2013), suggesting that there was a gradient in this direction, albeit a gentle one in this platform area, that resulted in little sediment transport to the south. In support of this idea, the minor deltaic sandbodies in the Yoredale Group that prograded from the north become proportionally much thinner within the cycles' more southerly development on the Askrigg Block, a trend that has been attributed to a structurally 'positive tendency' in this area (Wilson, 1960).

In addition to the calcarenite/calcisiltite lobes, the mudrock lithologies of the Bowland Shale also have a substantial carbonate content (MLF 2 and MLF 3). The laminated mudstones of MLF 3 have been identified in previous studies [e.g. fig. 16e in Clarke *et al*. (2018) and Facies B in Emmings *et al*. (2020a)] and interpreted as the product of low-density turbidity currents (Clarke *et al*., 2018, p. 299; Emmings *et al*., 2020a, p. 272). However, depositional processes responsible for the more massive facies of MLF 2 are challenging to determine. Some pelagic components may be present (e.g. the clay content and organic filaments), but the silt grade carbonate material, distributed throughout the facies, is unlikely to have settled from the water column because silt-grade grains (*ca* 20–62 µm; see Fig. 16B and C) do not remain in suspension for long (fall velocities in the range of tenths of a millimetre to millimetres per second; Gibbs *et al*., 1971). Potentially the massive nature of MLF 2 beds may be due to homogenization by intense bioturbation, but burrows are not seen. A bioturbated origin seems more likely for MLF 1, which shows occasional burrow mottling, and MLF 4, which both contain larger, unfragmented bioclasts which are likely to be *in situ* benthos.

In their study of the Bowland Shale, Emmings *et al*. (2020a) identified examples of MLF 2, which were mostly assigned to their Facies B and C, and attributed them to hemipelagic deposition and "small density flow events". The clay and organic content may be of hemipelagic origin but it co-occurs with fine calcareous detritus. Much of this calcareous material is less than 50 microns in size, and it could have been shed into the Bowland Basin via suspension clouds of fine sediment sourced from surrounding carbonate platforms. However, a few carbonate grains are larger, up to 0.5 mm and occasionally up to 2.0 mm in size. These are likely too large to have been transported by suspension clouds, therefore, the authors suggest that beds of MLF 2 record deposition from fine-grained, low-strength debris flows (cf. Talling *et al*., 2012), with their poor sorting, and 'floating' silt grains, being evidence of this transport process. The lack of bed contacts in MLF 2 makes the size of individual flow events difficult to ascertain.

Whatever the depositional process of MLF 2, it is likely that the carbonate platform on the Central Lancashire High supplied the calcarenites/calcisiltite bodies in the Bowland Basin and a significant proportion of the fine-grained sediment too (Fig. 18A). The isopach maps of the Bowland Shale carbonate bodies, showing their restriction to the south of the basin (Fig. 8), support this assertion. The Berwick Limestone (E_{1a} subzone) is the youngest carbonate unit in the basin, possibly because accelerated subsidence in the later Pendleian outpaced carbonate aggradation resulting in Bowland Shale onlapping the Central Lancashire High (Kirby *et al.,* 2000; Waters *et al*., 2020).

Finally, there are the enigmatic CLF 4 beds, which typically occur interbedded with MLF 4. In some cases, the limestone beds appear to be diagenetically recrystallized examples of CLF 3 (Fig. 13F), but others resemble aragonite fans that were widespread on anoxic seafloors in the Early Triassic (e.g. Woods *et al*., 2007). The Bowland Shale examples are much smaller (crystals are <1 mm height) – the fans are not visible to the naked eye – whilst many of the Early Triassic examples can reach 30 cm thickness with crystal laths of similar scale. However, the Bowland Shale examples show the same distinctive radial structure with long axes orthogonal to bedding (Fig. 13D). Euxinic conditions within the Bowland Basin may have been sufficiently alkaline to occasionally allow direct carbonate precipitation on the seafloor, probably originally as aragonite laths that have converted to calcite.

The prolonged development of anoxic–euxinic waters in the Bowland Basin over a period of *ca* 10 million years clearly did not impact carbonate productivity on the Askrigg Block carbonate platform, whilst abundant carbonate productivity on the Central Lancashire High platform persisted until late in Bowland Shale depositional history. This contrasts with many examples that show the shut-down of shallow-water carbonates by onlapping black shales (e.g. Petrash *et al*., 2016). A clear example is close at hand in the contemporaneous Dublin Basin 250 km to the west of the Bowland Basin where progressive carbonate platform collapse in the Brigantian saw the expansion of deep-water, organic-rich shale deposition. By the Pendleian, shales of the Donore Formation covered the entire region (Pickard *et al*., 1994). Carbonate aggradation was presumably unable to keep pace with subsidence rates in the Dublin region. In other examples, carbonate shut-down is attributed to poisoning by upwelling euxinic waters (Caplan & Bustin, 1999; Li *et al*., 2022). This did not occur during Bowland Shale deposition even though euxinic black shales developed in close proximity to the well-oxygenated facies of the Yoredale Group (Fig. 6). This suggests a sharp demarcation between euxinic and oxic deposition and the likelihood of a stable density interface within the upper water column that protected the shallow waters from sulphidic incursions (Li *et al*., 2022).

Siliciclastic depositional process and sediment source

The sandstone facies of the Pendleside Sandstone are considered to be a turbidite sandbody (Clarke *et al*., 2018), an interpretation supported by our isopach map for this Member. This shows a broad outcrop occupying the central portion of the basin, and a narrow eastern development that likely records the feeder channel (Figs 7 and 18B), which implies that clastic sediment was reaching the basin via a route that lay east of the Harrogate Basin. Clarke *et al*. (2018) suggested that sandstones with abraded bioclasts (facies CSF 2 herein) found in the Pendleside Sandstone could record marine reworking in a shelfal source area before sediment was transported into the basin. Alternatively, the authors propose that the bioclasts may have been shed off the northern end of the Central Lancashire High into the Pendleside Sandstone feeder channel and incorporated with the clastic sediment being transported westwards into the basin.

The lenticular, organic-rich mudstone of MLF 4 dominates the Pendleian-aged Bowland Shale, but is also common in the older Bowland Shale (Fig. 15), and in black shales generally (e.g. Könitzer *et al*., 2014; Li *et al.,* 2020; Peng, 2021). Its origin has been the subject of considerable study, especially the component clay lenses which are often considered to be intraclasts (Könitzer *et al*., 2014; Laycock *et al*., 2017; Schieber *et al*., 2010; Emmings *et al*., 2020a; Newport *et al.,* 2020), transported to the depositional site either as bedload (Könitzer *et al.,* 2014; Peng, 2021) or within low strength, cohesive debris flows (Boulesteix *et al.,* 2019; Wei & Swennen, 2022). This study interprets the components of MFL 4 (pelagic fossils, organic lenses, syngenetic framboids and clay lenses, all encased in a matrix of clay) to record hemipelagic deposition. Clearly the biogenic material settled through the water column, whilst the lenses were likely pelagic faecal pellets, which are responsible for substantial hemipelagic fallout in modern oceans (Turner, 2015; Fig. 18).

Such pellets vary in size over a considerable range, from *ca* 10 μm to several millimetres (Gowing & Silver, 1985; Fowler & Knauer, 1986), a range comparable with that seen in the Bowland Shale. Copepod pellets are especially important today and occur in sizes ranging from 200 to 400 μm (Turner, 2015). Modern pellets are typically composed of a mixture of terrigenous detritus (clay minerals and wind-blown silt) (Dunbar & Berger, 1981; Cuomo & Bartholomew, 1991), and often biogenic particles such as diatoms and coccoliths (Ploug & Iverson, 2008). The latter groups did not evolve until the Mesozoic, therefore, the pellets of the Palaeozoic are only composed of clay and silt (cf. Macquaker *et al*., 2010). Sinking marine snow (phytodetritus aggregates) is also important for the export of suspended material to the seafloor (Turner & Ferrante, 1979; Turner, 2015) but is unlikely to account for the organic-lean clay lenses of the Bowland Shale. A marine snow origin is more likely for the organic filaments found between the lenses. Further evidence for the pelagic origin of MLF 4 comes from the sediment between the clay lenses; this includes the very thin planktonic larval shells of bivalves, which are dominantly unfragmented and aligned parallel to bedding (Fig. 17A). These are likely to have settled through the water column. Transport and deposition from turbulent gravity currents would fragment such shells, whilst transport in cohesive mud-rich flows with matrix strength would result in shells at high angles in the sediment and even perpendicular to bedding (Peng, 2021; Peng *et al*., 2022).

Pyrite framboids are abundant in the Bowland Shale, especially in MLF 4, where they are small (average diameter *ca* 5 – 6 μm), suggesting that they formed at the redox boundary within the water column before sinking to the seabed where no further framboids form: a situation pertaining in the modern Black Sea (Li *et al*., 2024). Notably, framboids are absent from within the clay lenses (Fig. 17E), suggesting that the lenses formed within the water column above the site of framboid formation at the chemocline. Syngenetic framboids do not form below the redox boundary (Wilkin & Barnes, 1997), hence their absence from the clay lenses that had settled to the seabed.

Emmings *et al*. (2020a p. 272) suggested an alternative origin for MLF 4 with the clay lenses being "mud clasts sourced from upslope scour by tidal and/or wind shear and delivered [to the basin] via bedload currents". The tidal range is, however, predicted to have been very small for the Upper Carboniferous basins (Wells *et al*., 2005), ensuring that tidal currents are unlikely to have been a source of erosive power, in keeping with the general absence of tidal deltaic characteristics in these basins (Collinson, 1988). Having noted this lack of evidence for tidal deposits, Emmings *et al*. (2020a) then discuss the possibility of tidal amplification in this basin. Those authors further argue for enhanced amplification of bottom currents, and erosion of upslope muds, on the basis of tempestite deposits. These tempestites are interpreted on the basis of mud caps (T_E) and 'deformation' of basal silty laminae, but neither are diagnostic criteria (Schieber, 1986, 2016). The source of clay intraclasts is stated to be from prodelta muds ponded in the Craven Fault Belt area between the North Craven and South Craven faults (Emmings *et al*., 2020a, Fig. 17). However, this area saw basinal (not prodelta) mudrock deposition during formation of the Bowland Shale. Furthermore, for much of the depositional history, a carbonate platform lay to the north and so was unlikely to source clay intraclasts (Fig. 6). Clay lenses are present in both MLF 2 and MLF 4 and first appear in the Asbian mudstones of the Bowland Basin (Fig. 15). The Askrigg Block was a carbonate platform during the Asbian, isolated from the Bowland Basin to the south by the Cracoe reef belt (Kirby *et al*., 2000; Waters *et al*., 2017b). Clearly no clay intraclasts could have been supplied to the basin from such a hinterland. Even during the Brigantian, mudrocks are subordinate amongst the lithologies of the Yoredale Group on the Askrigg Block.

Emmings *et al*. (2020a) supported their bedload transportation theory with illustrations of clasts showing imbrication (see also Könitzer *et al.,* 2014, fig. 5c), but their images are not compelling. The examples of 'imbrication' show incorrect orientations and stacking relationships relative to flow or consist of an isolated pair of clasts rather than a bedload layer. Transport of clay lenses by bedload, would be expected to lead to bedload layers at least several grain-diameters in thickness (Gomez, 1991) without organic material in between them. Furthermore, bedload transport should produce lenses that are much better sorted (e.g., Kuenen & Humbert, 1969; Komar, 1985) and, given the observed size range, the lenses should show tractional structures such as upper-stage plane beds or ripples, (e.g., Arnott & Hand, 1989; Baas *et al*., 2021a). Emmings *et al*. (2020a) also argue that equant grains, stacking of lenses, the presence of compound lenses-within-lenses, features identified as microbial mats such as roll-over textures, and an observed cyclicity in lens size, also suggest an intraclast origin. This study assesses each feature in turn: (i) equant grains are incompatible with bedload transport and imbrication, and the examples noted are probably calcispheres or radiolarians infilled with either calcite or phosphate crystals; (ii) no arguments are provided for why the interpreted stacking of lenses suggests intraclasts; (iii) the compound lenses have very irregular shapes that suggest an absence of sediment transport because there is no rounding of any kind; (iv) the illustrated example is not reminiscent of roll-up fabrics which are composed of rolled up and compacted organic matter without incorporated lenses; and (v) the cyclicity is based on 23 thin-section locations at a single spatial position, covering four marine band cycles, one of which does not fit the claimed cyclicity, and three of which are supported by just three thin section locations; the claim for cyclicity thus lacks robustness.

Emmings *et al*. (2020a) argued that the lenses are rip-up clasts and that they were derived from a source area of "shelfal, mud-rich successions" where the prevailing oxic conditions did not support pyrite formation. On arrival on the basin floor, it is suggested that the consolidated nature of the intraclasts ensured that their low permeability "potentially limited infiltration by syngenetic and/or diagenetic (sulphidic) pore-fluids" (Emmings *et al*., 2020b p. 284), hence the absence of framboids from within the lenses. However, the highly compacted/flattened nature of the lenses suggests that they were water-rich when deposited rather than being rip-up clasts that were consolidated to a level where solute infiltration was not possible.

It is of course possible that there are multiple origins for the clay lenses, both as reworked clasts and faecal pellets, and that a broad range of depositional processes is responsible for mudrock accumulation. However, a key issue for a model in which black shale deposition is dominated by transported intraclasts lies in its significance for geochemical studies. Many, if not most, black shale facies are identical to MLF 4, and they are considered to provide a reliable record of basinal redox conditions, but if the majority of constituent clasts are transported from the shallow-water basin margin, then this assumption is wrong. As is argued above, the fabric of MLF 4 suggests the clay lenses settled through the water column, together with the associated clay matrix, tiny framboids, organic filaments (marine snow) and pelagic bioclasts (e.g. planktonic bivalve larval shells, goniatites, radiolarians and calcispheres). Consequently, the Bowland Shale is likely to provide an *in situ* record of redox conditions as assumed in geochemical studies of black shale formations generally.

Diagnostic criteria for hemipelagic faecal pellets versus transported rip-up clasts in organic-rich mudstones

Sufficient diagnostic criteria are available to distinguish between faecal pellet and rip-up clast origins for clay lenses in organic-rich mudstones (Table 2). Application of these criteria in future studies should allow the significance of the erosion and transportation as a mechanism for mudrock deposition to be evaluated. The deposition of silt to coarse sand grade clay lense rip-up clasts from turbidity currents or debris flows is distinctly different origin compared with settling of pellets. This has broad implications for basin models, sediment transport processes and provenance of mudrocks. As noted above, it is especially important when interpreting basin redox conditions from geochemical data derived from clay lense-rich black shales. Comparison of redox proxies from clay lense-rich and lense-poor black shales should prove valuable.

Eustatic influence?

Deep-water carbonate systems are typically fed from adjacent carbonate platforms during highstand or transgression when productivity is high: a phenomenon known as highstand shedding (e.g. Reijmer *et al.*, 2015; Peng, 2021). In contrast, clastic turbidite systems are traditionally formed during lowstand conditions when base level fall ensures clastic sediment is transported to the shelf break. During Bowland Shale deposition carbonate fans formed in the Bowland Basin around the Asbian/Brigantian boundary ($P_{1a\text{-}b}$), in the early Brigantian ($P_{1b\text{-}c}$) and in the early Pendleian (E_{1a}), whilst a siliciclastic turbidite system formed in the mid-Brigantian (around the P_1/P_2 boundary) and Bowland Shale deposition was terminated in the late Pendleian (E_{1c}) in the Bowland Basin when the substantial Pendle Grit turbidite system arrived. These occurrences do not fit closely with purported base-level changes in the surrounding area. The Asbian/Brigantian boundary is marked by a major palaeokarst surface in platform carbonates in the region, which is considered to be a third-order sequence boundary and one of the few possible eustatic signatures of the interval (Manifold *et al.*, 2021). This lowstand coincides with the formation of the Ravensholme Limestone within the

Bowland Basin, indicating that base-level fall was insufficient to expose the Central Lancashire High and shut down carbonate productivity on this platform. In contrast, the early Pendleian (E_{1a}) saw the development of black shales in many European basins, suggesting a major transgression (Clarke *et al*., 2018). This interval coincides with the final carbonate fan development in the Bowland Basin, which could indicate highstand shedding. However, the other carbonate fans in the Bowland Basin do not correlate with transgressive episodes and the E_{1a} development may be purely coincidental. The notion of an E_{1a} eustatic transgression is, in any case, highly questionable because there was no associated expansion of Bowland Shale deposition in the region, and neither is there evidence for back-stepping on the Askrigg Block (Fig. 4). Other factors, notably tectonism and development of sediment transport routes, were likely to be much more critical than eustasy in controlling the supply of sediment (both siliciclastic and carbonate) to the Bowland Basin. Recent studies have also challenged the received wisdom that eustasy affected deposition of the distinctly cyclic Yoredale Group on the Askrigg Block and instead favoured autogenic controls (Manifold *et al*., 2020, 2021). The absence of synchrony between basinal facies development and cyclicity on surrounding shelf areas supports the contention of Manifold and colleagues.

CONCLUSIONS

This analysis of depositional history of the Bowland Basin aimed to examine the diverse controls on deposition and facies evolution within the basin. Tectonics, sediment supply (especially productivity on surrounding carbonate platforms) and siliciclastic sediment access routes to the basin were all clearly important in defining basin geometry and facies development. However, there is no evidence that eustasy influenced deposition in the Bowland Basin; calciturbidite fan and siliciclastic turbidite systems show no clear relationship with regional base-level changes. The principal origin of allochthonous carbonate detritus lay in the south-east of the Bowland Basin on a small isolated carbonate platform (Central Lancashire High) on which productivity remained high until late in the history of Bowland Shale accumulation. The presence of intensely anoxic basin waters in the adjacent basin did not suppress carbonate production on this platform and its ultimate demise may instead relate to an episode of rapid subsidence. In contrast, the large carbonate platform to the north of the Bowland Basin (Askrigg Block) shed little carbonate detritus, perhaps because transport directions were to the north away from the Basin.

Arenaceous siliciclastic sediment reached the basin from an adjacent basin to the east through a narrow fault-defined conduit. Turbidite deposition within the basin was controlled by intrabasinal topography, which also caused the reflection of carbonate-laden turbidity currents sourced from a platform to the south east. The resulting combined flows produced calciturbidites with swale-like and hummock-like bedforms. The finer-grained strata of the Bowland Shale record a diverse range of depositional processes. During the early phase of Bowland Shale accumulation, widespread calcareous shales were developed throughout the basin. These are composed of fine-grained, highly abraded bioclastic debris. As noted above, the coarser calcarenitic material was sourced from the Central Lancashire High and it seems likely that the finer carbonate fraction also came from this source via two styles of sediment gravity flow. Laminated, calcareous silty mudstones are likely the product of deposition from small-scale turbidity currents, but unlaminated, massive mudstones are also common. These contain floating bioclasts and were likely deposited from low-strength debris flows.

Hemipelagic deposition during the early phase of Bowland Shale deposition was of secondary importance compared with the sediment-gravity flows shedding from an adjoining carbonate platform. The younger Bowland Shale, by contrast, records more uniform black shale deposition that the authors argue is the product of hemipelagic settling. The dominant lithology is an organic-rich mudstone with a lenticular fabric consisting of clay lenses (0.05 — 0.4 mm in width) floating in a matrix of clay, organic matter filaments, larval shells and pyrite framboids. This study interprets the lenses to be faecal pellets derived from the water column, together with other pelagic components with which they are intimately interbedded (e.g. marine snow, syngenetic framboids and planktonic larval stages of marine organisms). Such clay lenses in mudrocks are commonplace and frequently interpreted to be rip-up clasts that have been transported, either as bedload or in dilute density currents. The lack of a shelfal mud source argues against this origin for the Bowland Shale lenses, because the Bowland Basin was surrounded by carbonate platforms for much of its depositional history. A rip-up clast origin is also not supported by the presence of the well-preserved ultra-thin shells of planktonic origin in the Bowland Shale euxinic facies. The notion that black shales are the result of the transport and accumulation of reworked mudstone intraclasts (e.g. Schieber *et al*., 2010; Li *et al*., 2021; Peng, 2021) may be correct in some cases, but it challenges the accepted wisdom in geochemical studies that use black shales as a repository of the *in situ* redox signal within the basin. Criteria are provided to distinguish between faecal pellet from hemipelagic settings, with rip-up clast origins for clay lenses that will hopefully prove useful in future studies.

ACKNOWLEDGEMENTS: Our gratitude goes to Dr. Kaixuan Ji, Yuxuan Wang, Dr. Yafang Song, Dr. Zhen Xu and Dr. Jed Atkinson who provided valuable help during fieldwork. We thank the editor Jaco Baas, associate editor Rick Sarg, and reviewers P. Burgess, J. Peng, C. Waters and J. Emmings for comments on this manuscript. This study is financially supported by the National Natural Science Foundation of China (grants no. 41821001)

CONFLICT OF INTEREST

We declare that we do not have any commercial or associative interest that represents a conflict of interest in connection with the work submitted

DATA AVAILABILITY STATEMENT

The authors confirm that the data supporting the findings of this study are available within the article. Research data are not shared in any data repository.

FIGURE CAPTIONS

Fig. 1. (A) Global palaeogeography during the Mississippian showing location of the study region. (B) Regional palaeogeography showing the location of the Bowland Basin amongst a series of fault-bounded block-and-basins. (C) Stratigraphy of the Bowland Basin. PL Pendleside Limestone Formation; HL Hodderense Limestone Formation; PSM Pendleside Sandstone Member; RLM Ravensholme Limestone Member; PLM Park Style Limestone Member. After Earp *et al*. (1961), Aitkenhead *et al*. (1992) and Waters *et al*. (2009). Abbreviated stages are the Serpukhovian (Serpukhov) and Holkerian (Hol.).

Fig. 2 Study area in the Bowland Basin, Craven Fault Belt (between the South and North Craven Faults) and the southern Askrigg Block and location of study sections (see Table 1). MCF – Mid Craven Fault, CC – Cow Close, CH – Clough Head Beck, DH – Dinckley Hall, SF – Dob Dale Beck, DB – Dobson’s Brook, FF – Fountain Fell, FL – Fell Lane, LT – Linton Church, LB –

Leagram Brook, LC – Light Clough, MC – Moor Close Gill, RH – River Hodder, SS – School Share, SM – Smelthwaite Farm, SC – Swardean Clough, TLC – Tory Log Clough.

Fig. 3 Isopach map of the Asbian-Brigantian-aged Bowland Shale Formation showing the influence of structural features (Craven faults and the Slaidburn Anticline) on sediment thickness. Dots represent locations of thickness data, primarily derived from the records of Geological Survey memoirs.

Fig. 4 Correlation panels for Bowland Shale sections along two north-east/south-west transects from the margins to the centre of the Bowland Basin (see Fig. 2 and Table 1 for outcrop details). RSM Ravensholme Limestone Member; PSM Pendleside Sandstone Member; MLF mudstone lithofacies; CLF carbonate lithofacies; CSF siliciclastic sandstone lithofacies (see lithofacies section in the main text).

Fig. 5 Sedimentary logs of the lower parts of the Bowland Shale showing the diverse range of facies types developed at this level. (A) Basinal Tory Log Clough (TLC) section, ranging in age from the late Asbian – Brigantian (cf. Fig. 4), showing numerous limestone interbeds (this is a typical style of development of the Ravensholme Limestone Member). The strata below 73 m height (not shown) belong to the underlying Pendleside Limestone Formation; the topmost bed at 110 m height marks the erosive-base of the Pendleside Sandstone Member. (B) Sedimentary log of the basalmost Bowland Shale developed at the Fell Lane section (basal Brigantian age, cf. Fig. 2) showing interbeds of several limestone facies, notably boulder-bearing beds (CLF 1) with typical Bowland Shale dark mudstone lithologies. Note that MLF 3 and MLF 4 mudstones cannot be distinguished without thin section study.

Fig. 6 Cross-section from the southern margin of the Askrigg Block to the southern-most outcrops of the Bowland Basin (see line of section in Fig. 2), showing the thick development of the Pendleside Sandstone in the lower part of the Bowland Shale, and levels of main limestone units and the laterally equivalent lithologies of the Yoredale Group.

Fig. 7 Thickness variations in Pendleside Sandstone in the Bowland Basin. Isopachs are dashed where data density is low. Sections where thicknesses have been measured denoted with a • and elsewhere thicknesses have been estimated from the maps of the British Geological Survey.

Fig. 8 Isopachs for carbonate bodies developed in the Bowland Shales and location of localized, limestone boulder beds. The elongate nature of the carbonate bodies is the simplest way of honouring the data. In the Berwick Limestone where data are sparse, the interpretation relies on that of the other two carbonate members.

Fig. 9 Isopach map of the Pendleian-aged Bowland Shale Formation in the Bowland Basin and Craven Fault Belt area showing principal depocentres adjacent to bounding faults.

Fig. 10 Field photographs of carbonate beds in the Bowland Shale. (A) Coarse calcirudite bed (CLF 1), dominantly composed of crinoid columnals, P_{1b} subzone, Fell Lane section. The yellow disc is 14 mm in diameter. (B) Coarse calcirudite bed (CLF 1), loose block, showing large tabular clasts of Bowland Shale, P_{1b} subzone, Fell Lane section. Yellow disc is 14 mm in diameter. (C) Loose block of CLF 2 bed showing massive, graded lower part (T_a division) of coarse calcarenite grading upwards into fine-grained, laminated strata (T_b division), B_{2b} subzone, Dobson’s Brook section. (D) CLF 2 bed displaying a broad hummock (yellow arrows denote base), whilst overlying (topmost) bed is graded, and nearly 1 m thick, B_{2b} subzone, Dobson’s Brook section. (E) limestone bed (CLF 4) displaying hummock-like topography, E_{1b} subzone, Dinckley Hall section. Yellow notebook is 20 cm in length. (F) Block of CLF 2, a hummock-like bedform with laminae showing a simple thickening of beds from right to left. Internally, minor soft sediment deformation or possibly small oscillatory structures are developed, B zones, Dobson’s Brook.

Fig. 11 Thin section photographs of limestone facies from the Bowland Shale. (A) CLF 1 coarse calcirudite with crinoid bioclasts and wackestone intraclast, P_{1b} subzone, Fell Lane section. (B) CLF 1 coarse calcirudite with large brachiopod shell with broken spine attached. The matrix shows a mix of micrite and sparry patches, P_{1b} subzone, Fell Lane section. (C) CLF 2 coarse calcarenite/grainstone dominated by peloids, with foram and crinoid bioclasts, basal P_{1a} subzone, Tory Log Clough section. (D) CLF 2 coarse calcarenite composed of peloids, crinoid columnals (showing micrite envelopes), calcareous algae (*Koninckopora,* outlined) and forams. B_{2a} subzone, basal Lower Bowland Shales, Dobson’s Brook. (E) CLF 2 calcarenite dominated by peloids, intraclasts with micrite envelopes and rarer quartz grains, B_2 zone, basal-most Lower Bowland Shale, Swardean Clough. (F) CLF 2 fine calcarenite/ pack-grainstone with peloids, coated grains, forams and possible micritised brachiopod shells, B_2 zone topmost bed of the Pendleside Limestone, immediately below base of Lower Bowland Shale, Swardean Clough.

Fig. 12 Evolving composition of allochthonous carbonates (CLF 2) found within the Asbian-Brigantian in the Bowland Basin. River Hodder data are from the Pendleside Limestone, all other data/the rest are from the Bowland Shale. The three most abundant clast types are displayed whilst others are included as ‘other bioclasts’. There is a broad transition within the basin from peloid-dominated to crinoid-dominated carbonates, the exception being the ultra-condensed Smelthwaite Farm section where peloidal carbonate dominates throughout.

Fig.13 Thin section photographs of limestone facies from the Bowland Shale. (A) CLF 3, calcisiltite with a fragment of mollusc skeletons showing prismatic structure, P_{1b} subzone, Fell Lane. (B) CLF 3 calcisiltite with spar-filled ostracod, P_{1b} subzone, Fell Lane. (C) CLF 4 micritic limestone displaying wavy lamination partially recrystallized to microspar, uppermost E_{1a} subzone, Dinckley Hall. (D) CLF 4 Microspar consisting of laths/stumpy prisms orientated vertically and showing a weak radial or fan-like arrangement, basal P_{1c} subzone, Smelthwaite Farm. (E) CLF 5, ostracod and crinoids in wackestone, basal P1a subzone, Smelthwaite Farm. (F) CLF 3 bioclastic wackestone bearing calcispheres and a thin-shelled bivalve, B_{2b} subzone, Dobson’s Brook.

Fig. 14 Thin section photographs of clastic sandstone lithofacies from the Bowland Shale.
(A) CSF 1 well sorted, fine sandstone seen in cross-polars, P_{1d} subzone, Tory Log Clough. (B) CSF 1 medium-fine grained sandstone with poor sorting, lower E_{1b} subzone, Dinckley Hall. (C) CSF 2, bioclast-rich sandstone containing brachiopod fragments (central), crinoid fragments (yellow arrows) and a foram (yellow circle, *Archaediscus*), basal P_{1d} subzone, Tory Log Clough. (D) CSF 2, bioclast-rich sandstone with forams (yellow circle, *Archaediscus*), basal P_{1d} subzone, Tory Log Clough.

Fig. 15 Stratigraphic variation of mudrock facies in selected Bowland Shale outcrops showing the increasing importance of organic-rich mudstones with abundant clay lenses (MLF 4) in younger strata at the expense of more carbonate-rich mudrock facies. HOL – Holkerian.

Fig. 16 Thin section and scanning electron microscope (SEM) photographs of mudrock facies from the Bowland Basin. (A) MLF 1 homogenous mudstone with mollusc skeletons showing prismatic structure and partial pyritic replacement, B_2 zone, basal Bowland Shale, Tory Log Clough. (B) MLF 2 calcareous, silty mudstone with common organic filaments, topmost Pendleside Limestone, B zone, Swardean Clough. (C) MLF 2 calcareous, silty mudstone with common bioclast fragments, B_{2a} subzone, basal lower Bowland Shale, Dobson's Brook. (D) MLF 2 SEM image showing abundant carbonate grains (light grey), clay minerals (dark grey), organic matter (black) and pyrite (bright colour) in the form of small, spherical framboids and a pyrite lens incorporating carbonate clasts, $P_{1b\text{-}P1c}$ boundary, Smelthwaite Farm. (E) MLF 3 laminated, calcareous mudstone consisting of carbonate-rich and clay rich laminae, P_{1a} subzone, Swardean Clough. (F) MLF 3 laminated, calcareous mudstone consisting of carbonate-rich laminae composed of angular calcisilt (fragmented bioclasts?) with clay and organic-rich laminae, uppermost P_{1a} subzone, Swardean Clough.

Fig. 17 Thin section and scanning electron microscope (SEM) photographs of lenticular, organic-rich mudrocks, MLF 4, from Dinckley Hall. (A) Example showing thin, articulated bivalve prodissoconch (yellow arrow), basal E_{1a} subzone. (B) Example with scattered radiolarians (arrowed), P_{2b} subzone. (C) Example showing typical clay lens-rich layer fabric and a homogenous lamina consisting of clay and organic matter (arrows denote the base), mid E_{1a} subzone. (D) Example with phosphatic nodules (largest example arrowed), mid E_{1a} subzone. (E) SEM image showing a clay lens lacking framboids (delineated by arrows) in a matrix with abundant small framboids (bright spots), lower E_{1a} subzone. The lens is highly mechanically compacted and squeezed, which indicate the primary particle was soft, ductile, and water-rich. (F) Example with several ammonitellas (larval goniatites) in a matrix rich in framboids and clay lenses, basal P_{1c} subzone.

Fig. 18 Schematic models for the deposition of the Bowland Shale in the Bowland basin: (A) illustrating the diverse deposition processes of different lithofacies mentioned in the text, showing a combination of pelagic and hemipelagic settling and shedding of carbonate detritus, especially from the Central Lancashire High; (B) depositional model for the Pendleside Sandstone, sourced from a narrow channel in the north-east of the basin with the down-dip development showing deflection around the intrabasinal high formed by the Slaidburn Anticline.

Table 1: Field locations in the Craven Basin and Craven Fault Belt (cf. Fig. 2).

Table 2: Summary of criteria for distinguishing between hemipelagic faecal pellets and transported intraclast origin for the clay lenses commonly encountered in mudrocks.

REFERENCES

Aitkenhead, N., Bridge, D.M., Riley, N.J. and **Kimbell, S.F** (1992) Geology of the Country Around Garstang: Memoir for 1: 50,000 Geological Sheet 67 (England and Wales).

Algeo, T.J., Heckel. P.H., Maynard, J.B., Blakey, R.C. and **Rowe, H.** (2007) Modern and ancient epeiric seas and the super-estuarine circulation model of marine anoxia. In: *Dynamics of Epeiric Seas* (Eds. Pratt, P.R. and Holmden, C.), Geol. Assoc. Canada Spec. Paper, 48, 7-37.

Andrieu, S., **Krencker, F.N.** and **Bodin, S.** (2022) Anatomy of a platform margin during a carbonate factory collapse: implications for the sedimentary record and sequence stratigraphic interpretation of poisoning events. *J Geol. Soc. London*, **179**, jgs2022-005.

Arnott, R.W.C. and **Hand, B.M.** (1989) Bedforms, primary structures and grain fabric in the presence of suspended sediment rain. *J. Sed. Res.*, **59**, 1062–1069.

Arthurton, R.S. (1984) The Ribblesdale fold belt, NW England—a Dinantian-early Namurian dextral shear zone. In: *Variscan Tectonics of the North Atlantic Region* (Eds D.H.W. Hutton and D.J. Sanderson), *Geol. Soc. London Spec. Publ.*, **14**, 131–138.

Arthurton, R.S., **Johnson, E.W.** and **Mundy, D.J.C.** (1988) Geology of the country around Settle. Memoir of the British Geological Survey, Sheet 60 (England and Wales).

Baas, J.H., **Best, J.** and **Peakall, J.** (2021a) Rapid gravity flow transformation revealed in a single climbing ripple. *Geology*, **49**, 493–497.

Baas, J.H., **Tracey, N.D.** and **Peakall, J.** (2021b) Sole marks reveal deep-marine depositional process and environment: Implications for flow transformation and hybrid-event-bed models. *J. Sed. Res.*, **91**, 986–1009.

Black, W.W. (1940) The Bowland Shales from Thorlby to Burnsall, Yorkshire. *Trans. Leeds Geol. Ass.*, **5**, 308–321.

Black, W.W. (1950) The Carboniferous geology of the Grassington area, Yorkshire. *Proc. Yorks. Geol. Soc.*, **28**, 29–42.

Booker, K.M. and **Hudson, R.G.S.** (1926) The Carboniferous sequence of the Craven Lowlands south of the reef limestones of Cracoe. *Proc. Yorks. Geol. Soc.*, **20**, 411–438.

Boulesteix, K., **Poyatos-Moré, M.**, **Flint, S.S.**, **Taylor, K.G.**, **Hodgson, D.M.** and **Hasiotis, S.T.** (2019) Transport and deposition of mud in deep-water environments: Processes and stratigraphic implications. *Sedimentology*, **66**, 2894–2925.

Brandon, A., Aitkenhead, N., Crofts, R.G., Ellison, R.A., Evans, D.J. and **Riley, N.J.** (1998) Geology of the Country around Lancaster: Memoir of the Geological Survey of Great Britain for 1: 50 000 Geological Sheet 59 (England and Wales).

Caplan, M.L. and **Bustin, R.M.** (1999) Devonian-Carboniferous Hangenberg mass extinction event, widespread organic-rich mudrock and anoxia: Causes and consequences. *Palaeogeogr. Palaeoclimatol. Palaeoecol.*, **148**, 187–207.

Clarke, H., **Turner, P.**, **Bustin, R.M.**, **Riley, N.** and **Besly, B.** (2018) Shale gas resources of the Bowland Basin, NW England - A holistic study. *Petroleum Geoscience*, **24**, 287–322.

Collinson, J.D. (1988) Controls on Namurian sedimentation in the Central Province basins of northern England. In: *Sedimentation in a Synorogenic Basin Complex: The Upper Carboniferous of Northwest Europe* (Eds B.M. Besly and G. Kelling), pp. 85–101. Blackie, Glasgow.

Cooper, A.H. and **Burgess, I.C.** (1993) Geology of the country around Harrogate: Memoir for 1: 50, 0000 geological sheet 62 (England and Wales).

Cuomo, M.C. and **Bartholomew, P.R.** (1991) Pelletal black shale fabrics: their origin and significance. In: *Modern and Ancient Continental Shelf Anoxia* (Eds R.V. Tyson and T.H. Pearson), *Geological Society London Special Publications*, **58**, 221-232.

de Jonge-Anderson, I. and **Underhill, J.R.** (2020) Structural constraints on Lower Carboniferous shale gas exploration in the Craven Basin, NW England. *Petroleum Geoscience*, **26**, 303–324.

Demaison, G.J. and **Moore, G.T**. (1980) Anoxic environments and oil source bed genesis. *Org. Geochm.,* **2**, 9-31.

Dixon, E.E.L., and **Hudson, R.G.S.** (1931) A mid-Carboniferous boulder-bed near Settle. *Geol. Mag.*, **68**, 81-92.

Dunbar, R.B. and **Berger, W.H.** (1981) Fecal pellet flux to modern bottom sediment of Santa Barbara Basin (California) based on sediment trapping. *Geol. Soc. Amer. Bull.,* **92**, 212-218.

Dunham, K.C. and **Wilson, A.A.** (1985) Geology of the Northern Pennine Orefield, Volume 2. Stainmore to Craven. *Economic Memoir Br. Geol. Surv.,* Sheets 40, 41, 50 and parts of 31, 32, 51, 60 and 61, New Series.

Dżułyński, S. and **Walton, E.K.** (1965) *Sedimentary Features of Flysch and Greywackes*. Developments in Sedimentology 7, Elsevier, Amsterdam, 274 pp.

Earp, J.R., **Poole, E.G.** and **Whiteman, A.J.** (1961) Geology of the country around Clitheroe and Nelson. *HM Stationery Office*.

Emmings, J.F., **Davies, S.J.**, **Vane, C.H.**, **Moss-Hayes, V.** and **Stephenson, M.H.** (2020a) From marine bands to hybrid flows: Sedimentology of a Mississippian black shale. *Sedimentology*, **67**, 261–304.

Emmings, J.F., **Poulton, S.W.**, **Vane, C.H.**, **Davies, S.J.**, **Jenkin, G.R.T.**, **Stephenson, M.H.**, **Leng, M.J.**, **Lamb, A.L.** and **Moss-Hayes, V.** (2020b) A Mississippian black shale record of redox oscillation in the Craven Basin, UK. *Palaeogeogr. Palaeoclimatol. Palaeoecol.*, **538**, 109423.

Fowler, S.W. and **Knauer, G.A.** (1986) Role of large particles in the transport of elements and organic compounds through the oceanic water column. *Prog. Oceano*., **16**, 147-194.

Fraser, A.J. and **Gawthorpe, R.L.** (1990) Tectono-stratigraphic development and hydrocarbon habitat of the Carboniferous in northern England. In: *Tectonic Events Responsible for Britain's Oil and Gas Reserves* (Eds. Hardman, R.F.P. and Brooks, J.), *Geol. Soc. Spec. Publ.*, **55**, 49–86.

Gawthorpe, R.L. (1986) Sedimentation during carbonate ramp-to-slope evolution in a tectonically active area: Bowland Basin (Dinantian), northern England. *Sedimentology*, **33**, 185–206.

Gibbs, R.J., Matthews, M.D. and **Link, D.A.** (1971) The relationship between sphere size and settling velocity. *Journal of Sedimentary Petrology*, **41**, 7-18.

Gomez, B. (1991) Bedload transport. *Earth Sci. Rev.*, **31**, 89–132.

Gorsline, D.S., **Nava-Sanchez, E.** and **de Nava, J.M.** (1996) A survey of occurrences of Holocene laminated sediments in California Borderland Basins: products of a variety of depositional processes. In: *Palaeoclimatology and Palaeoceanography from Laminated Sediments* (Ed., Kemp, A.E.S.), *Geol. Soc. London Spec. Publ.*, **116**, 93–110.

Gowing, M.M. and **Silver, M.W**. (1985) Minipellets: A new and abundant size class of marine fecal pellets. *J. Mar. Res.*, **43**, 395-418.

Gross, D., **Sachsenhofer, R.F.**, **Bechtel, A.**, **Pytlak, L.**, **Rupprecht, B.** and **Wegerer, E.** (2015) Organic geochemistry of Mississippian shales (Bowland Shale Formation) in central Britain: Implications for depositional environment, source rock and gas shale potential. *Mar. Pet. Geol.*, **59**, 1–21.

Hallock, P. and **Schlager, W.** (1986) Nutrient excess and the demise of coral reefs and carbonate platforms. *Palaios*, **1**, 389–398.

Harms, J.C., Southard, J.B., Spearing, D.R. and **Walker, R.G.** (1975) *Depositional Environments as Interpreted from Primary Sedimentary Structures and Stratification Sequences*. Society for Sedimentary Geology (SEPM) Short Course 2**,** 161 pp.

Hennissen, J.A.I. and **Gent, C.M.A.** (2019) Total organic carbon in the Bowland-Hodder Unit of the southern Widmerpool Gulf: a discussion. *J. Pet. Sci. Eng.*, **178**, 1194–1202.

Hofstra, M., **Peakall, J.**, **Hodgson, D.M.** and **Stevenson, C.J.** (2018) Architecture and morphodynamics of subcritical sediment waves in an ancient channel–lobe transition zone. *Sedimentology*, **65**, 2339–2367.

Hudson, R.G.S. (1930) The Carboniferous of the Craven Reef Belt: The Namurian uncomformity at Scaleber, near Settle. *Proc. Geol. Assoc.*, **41**, 290-IN8.

Hudson, R.G.S. and **Mitchell, G.H.** (1937) The Carboniferous geology of the Skipton anticline. *Summary of Progress of the Geological Survey for 1935*, 1–45.

Jelby, M.E., Grundvåg, S.-A., Helland-Hansen, W., Olaussen, S. and **Stemmerik, L.** (2020) Tempestite facies variability and storm-depositional processes across a wide ramp: Towards a polygenetic model for hummocky cross-stratification. *Sedimentology*, **67,** 742-781.

Kane, I.A. (2010) Development and flow structures of sand injectites: The Hind Sandstone Member injectite complex, Carboniferous, UK. *Mar. Pet. Geol.*, **27**, 1200–1215.

Keavney, E., Peakall, J., Wang, R., Hodgson, D.M., Kane, I.A., Keevil, G.M., Brown, H.C., Clare, M.A. and **Hughes, M.J.** (2025) Unconfined gravity current interactions with orthogonal topography: Implications for combined-flow processes and the depositional record. *Sedimentology*, doi:10.1111/sed.13227

Kirby, G.A., Bailey, H.E., Chadwick, R.A., Evans, D.J., Holliday, D.W., Holloway, S., Hulbert, A.G., Pharaoh, T.C., Smith, N.J.P., Aitkenhead, N. and **Birch, B.** (2000) The structure and evolution of the Craven Basin and adjacent areas: subsurface memoir. Subsurface Memoir of the British Geological Survey, *Stationery Office*.

Komar, P.D. (1985) The hydraulic interpretation of turbidites from their grain sizes and sedimentary structures. *Sedimentology*, **32**, 395-407.

Könitzer, S.F., **Davies, S.J.**, **Stephenson, M.H.** and **Leng, M.J.** (2014) Depositional controls on mudstone lithofacies in a basinal setting: implications for the delivery of sedimentary organic matter. *J. Sed. Res.*, **84**, 198–214.

Krencker, F.N., **Bodin, S.**, **Hoffmann, R.**, **Suan, G.**, **Mattioli, E.**, **Kabiri, L.**, **Föllmi, K.B.** and **Immenhauser, A.** (2014) The middle Toarcian cold snap: Trigger of mass extinction and carbonate factory demise. *Glob. Planet. Change*, **117**, 64–78.

Kuenen, P.H. and **Humbert, F.L.** (1969) Grain size of turbidite ripples. *Sedimentology*, **13**, 253–261.

Laycock, D.P., **Pedersen, P.K.**, **Montgomery, B.C.** and **Spencer, R.J.** (2017) Identification, characterization, and statistical analysis of mudstone aggregate clasts, Cretaceous Carlile Formation, Central Alberta, Canada. *Mar. Pet. Geol.*, **84**, 49–63.

Leeder, M.R. (1988) Recent developments in Carboniferous geology: a critical review with implications for the British Isles and N.W. Europe. *Proc. Geol. Assoc.*, **99**, 73–100.

Li, S., **Zhu, R.K.**, **Cui, J.W.**, **Luo, Z.**, **Jiao, H.**, and **Liu, H.** (2020). Sedimentary characteristics of fine-grained sedimentary rock and paleo-environment of Chang 7 Member in the Ordos Basin: A case study from Well Yaoye 1 in Tongchuan. *Acta Sedimentol. Sinca*, **38**, 554- 570 (In Chinese with English abstract).

Li, S., **Wignall, P.B.**, **Poulton, S.W.**, **Hedhli, M.** and **Grasby, S.E.** (2022) Carbonate shut-down, phosphogenesis and the variable style of marine anoxia in the late Famennian (Late Devonian) in western Laurentia. *Palaeogeogr. Palaeoclimatol. Palaeoecol.*, **589**, 110835.

Li, S., **Wignall, P.B.** and **Poulton, S.W.** (2025) Co-application of rhenium, vanadium, uranium and molybdenum as pale-redox proxies: Insight from modern and ancient environments. *Chem. Geol.*, **674**, 122565.

Li, S., **Wignall, P.B.**, **Xiong, Y.** and **Poulton, S.W.** (2024) Calibration of redox thresholds in black shale: Insight from a stratified Mississippian basin with warm saline bottom waters. *Bull. Geol. Soc. Amer.*, **136**, 1266-1286, doi.org/10.1130/B36915.1

Li, Z., **Schieber, J.**, and **Pedersen, P.K.** (2021). On the origin and significance of composite particles in mudstones: Examples from the Cenomanian Dunvegan Formation. *Sedimentology*, **68**, 737-754.

Macquaker, J.H.S., **Keller, M.A.** and **Davies, S.J.** (2010) Algal blooms and “marine snow”: Mechanisms that enhance preservation of organic carbon in ancient fine-grained sediments. *J. Sed. Res.*, **80**, 934–942.

Manifold, L., **Hollis, C.** and **Burgess, P.** (2020) The anatomy of a Mississippian (Viséan) carbonate platform interior, UK: depositional cycles, glacioeustasy and facies mosaics. *Sediment. Geol.*, **401**, 105633.

Manifold, L., del **Strother, P.**, **Gold, D.P.**, **Burgess, P.** and **Hollis, C.** (2021) Unravelling evidence for global climate change in Mississippian carbonate strata from the Derbyshire and North Wales Platforms, Uk. *J. Geol. Soc. London*, **178**, jgs2020-106, doi: 10.1144/jgs2020-106

McGowan, D., Salian, A., Baas, J.H., Peakall, J. and **Best, J.** (2024) On the origin of chevron marks and striated grooves, and their use in predicting mud bed rheology. *Sedimentology*, **71**, 687-708, doi:10.1111/sed.13148.

Newport, S.M., **Jerrett, R.M.**, **Taylor, K.G.**, **Hough, E.** and **Worden, R.H.** (2018) Sedimentology and microfacies of a mud-rich slope succession: In the Carboniferous Bowland Basin, NW England (UK). *J. Geol. Soc. London*, **175**, 247–262.

Newport, S.M., **Hennissen, J.A.I.**, **Armstrong, J.P.**, **Taylor, K.G.**, **Newport, L.P.** and **Hough, E.** (2020) Can one-run-fixed-Arrhenius kerogen analysis provide comparable organofacies results to detailed palynological analysis? A case study from a prospective Mississippian source rock reservoir (Bowland Shale, UK). *Natural Resources Research*, **29**, 2011–2031.

Nöthig, E-M. and **von Bodungen, B.** (1989) Occurrence and vertical flux of probably protozoan origin in the southeastern Weddell Sea (Antarctica). *Marine Ecology Progress Series*, **56**, 281-289.

Peakall, J., **Best, J.**, **Baas, J.H.**, **Hodgson, D.M.**, **Clare, M.A.**, **Talling, P.J.**, **Dorrell, R.M.** and **Lee, D.R.** (2020) An integrated process-based model of flutes and tool marks in deep-water environments: Implications for palaeohydraulics, the Bouma sequence and hybrid event beds. *Sedimentology*, **67**, 1601–1666.

Peng, J. (2021) Sedimentology of the Upper Pennsylvanian organic-rich Cline Shale, Midland Basin: From gravity flows to pelagic suspension fallout. *Sedimentology*, **68**, 805–833.

Peng, J., Hu, Z., Feng, D. and **Wang, Q.** (2022) Sedimentology and sequence stratigraphy of lacustrine deep-water fine-grained sedimentary rocks: The Lower Jurassic Dongyuemiao Formation in the Sichuan Basin, Western China. *Marine and Petroleum Geology*, **164**, 105933.

Petrash, D.A., **Gueneli, N.**, **Brocks, J.J.**, **Méndez-Dot, J.A.**, **González-Arismendi, G.**, **Poulton, S.W.** and **Konhauser, K.O.** (2016) Black shale deposition and early diagenetic dolomite cementation during Oceanic Anoxic Event 1: The mid-Cretaceous Maracaibo Platform, northwestern South America. *Am. J. Sci.*, **316**, 669–711.

Pharaoh, T., **Haslam, R.**, **Hough, E.**, **Kirk, K.**, **Leslie, G.**, **Schofield, D.** and **Heafford, A.** (2020) The Môn–Deemster–Ribblesdale fold–thrust belt, central UK: a concealed Variscan inversion belt located on weak Caledonian crust. In: *Fold and Thrust Belts: Structural Style, Evolution and Exploration* (Eds Hammerstein, J.A., Di Cuia, R., Cottam, M.A., Zamora, G. and Butler, R.W.H.), *Geol. Soc. London Spec. Publ.*, **490**, 153–176.

Pickard, N.A.H., **Rees, J.G.**, **Strogen, P.**, **Somerville, I.D.** and **Jones, G.L.I.** (1994) Controls on the evolution and demise of Lower Carboniferous carbonate platforms, northern margin of the Dublin Basin, Ireland. *Geological Journal*, **29**, 93–117.

Ploug, H. and **Iversen, M.H.** (2008) Ballast, sinking velocity, and apparent diffusivity within marine snow and zooplankton fecal pellets: Implications for substrate turnover by attached bacteria. *Limnol. Oceanogr.*, **53**, 1878-1886.

Privat, A.M-L.J., **Hodgson, D.M.**, **Jackson, C.A-L.**, **Schwarz, E.** and **Peakall, J.** (2021) Evolution from syn-rift carbonates to early post-rift deep-marine intraslope lobes: The role of rift basin physiography on sedimentation patterns. *Sedimentology*, **68**, 2563–2605.

Privat, A.M-L.J., Peakall, J., Hodgson, D.M., Schwarz, E., Jackson, C.A-L. and **Arnol, J.A.** (2024) Evolving fill-and-spill patterns across linked early post-rift depocentres control lobe characteristics: Los Molles Formation, Argentina. *Sedimentology*, **71**, 1639-1685. doi: 10.1111/sed.13190

Reijmer, J. J.G., **Palmieri, P.**, **Groen, R.**, and **Floquet, M.** (2015). Calciturbidites and calcidebrites: Sea-level variations or tectonic processes? *Sed. Geol.*, **317**, 53-70.

Reijmer, J.J.G. (2021) Marine carbonate factories: Review and update. *Sedimentology*, **68**, 1729–1796.

Schieber, J. (1986) The possible role of benthic microbial mats during the formation of carbonaceous shales in shallow Mid-Proterozoic basins. *Sedimentology*, **33**, 521–536.

Schieber, J. (2016) Mud re-distribution in epicontinental basins – Exploring likely processes. *Mar. Pet. Geol*., **71**, 119–133.

Schieber, J., **Southard, J.B.** and **Schimmelmann, A.** (2010) Lenticular shale fabrics resulting from intermittent erosion of water-rich muds—interpreting the rock record in the light of recent flume experiments. *J. Sed. Res.*, **80**, 119–128.

Schlager, W. (1981) The paradox of drowned reefs and carbonate platforms. *Geol. Soc. Am. Bull.*, **92**, 197–211.

Talling, P.J., **Masson, D.G.**, **Sumner, E.J.** and **Malgesini, G.** (2012) Subaqueous sediment density flows: Depositional processes and deposit types. *Sedimentology*, **59**, 1937–2003.

Tinterri, R. (2011) Combined flow sedimentary structures and the genetic link between sigmoidal-and hummocky-cross stratification. *GeoActa*, **10**, 1–43.

Turner, J.T. (2015) Zooplankton fecal pellets, marine snow, phytodetritus and the ocean's biological pump. *Prog. Oceanogr.*, **130**, 205–248.

Turner, J.T. and **Ferrante, J.G.** (1979) Zooplankton fecal pellets in aquatic systems. *Bioscience,* **29**, 670-677.

Waters, C.N., and **Lowe, D.** (2013) Chapter 2: geology of the limestones, in Waltham, T. and Lowe, D. (eds.). Caves and Karst of the Yorkshire Dales, Volume 1: Great Hucklow, UK, *British Cave Research Association*, 11–28.

Waters, C.N., **Waters, R.A.**, **Barclay, W.J.** and **Davies, J.R.** (2009) A lithostratigraphical framework for the Carboniferous successions of northern Great Britain (onshore). British Geological Survey, 174 pp.

Waters, C.N., **Haslam, R.B.**, **Cózar, P.**, **Somerville, I.D.**, **Millward, D.** and **Woods, M.** (2017a) Mississippian reef development in the Cracoe Limestone Formation of the southern Askrigg Block, North Yorkshire, UK. *Proc. Yorks. Geol. Soc.*, **61**, 179–196.

Waters, C.N., **Cózar, P.**, **Somerville, I.D.**, **Haslam, R.B.**, **Millward, D.** and **Woods, M.** (2017b) Lithostratigraphy and biostratigraphy of the Lower Carboniferous (Mississippian) carbonates of the southern Askrigg Block, North Yorkshire, UK. *Geol. Mag.*, **154**, 305–333.

Waters, C.N., **Vane, C.H.**, **Kemp, S.J.**, **Haslam, R.B.**, **Hough, E.** and **Moss-Hayes, V.L.** (2020) Lithological and chemostratigraphic discrimination of facies within the Bowland Shale Formation within the Craven and Edale basins, UK. *Petroleum Geoscience*, **26**, 325–345.

Wei, W. and **Swennen, R.** (2022) Sedimentology and lithofacies of organic-rich Namurian Shale, Namur Synclinorium and Campine Basin (Belgium and S-Netherlands). *Mar. Pet. Geol.*, **138**, 105553.

Wells, M.R., **Allison, P.A.**, **Hampson, G.J.**, **Piggott, M.D.**, and **Pain, C.C.** (2005) Modelling ancient tides: the Upper Carboniferous epi-continental seaway of Northwest Europe. *Sedimentology*, **52**, 715-735.

Wignall, P.B. (1994) *Black shales.* Oxford University Press, Oxford, 320pp.

Wilkin, R.T. and **Barnes, H.L.** (1997) Formation processes of framboidal pyrite. *Geochim. Cosmochim. Acta*, **61**, 323–339.

Wilson, A.A. (1960) The Carboniferous rocks of Coverdale and adjacent valleys in the Yorkshire Pennines. *Proc. Yorks. Geol. Soc.*, **32**, 285-316

Woods, A.D., **Bottjer, D.J.** and **Corsetti, F.A.** (2007) Calcium carbonate seafloor precipitates from the outer shelf to slope facies of the Lower Triassic (Smithian-Spathian) Union Wash Formation, California, USA: Sedimentology and palaeobiologic significance. *Palaeogeogr. Palaeoclimatol. Palaeoecol.*, **252**, 281–290.

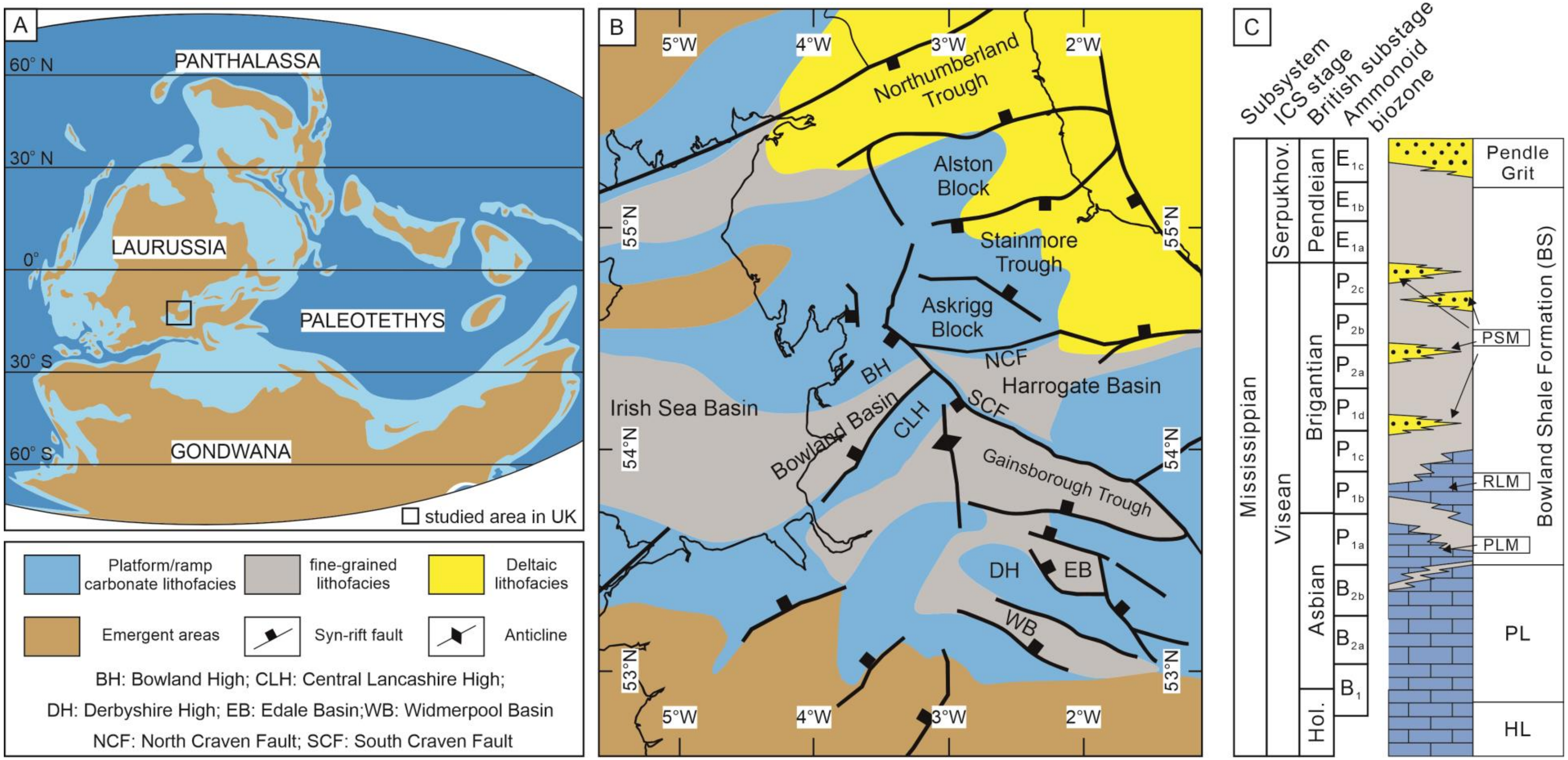

Fig. 1. (A) Global palaeogeography during the Mississippian showing location of the study region. (B) Regional palaeogeography showing the location of the Bowland Basin amongst a series of fault-bounded block-and-basins. (C) Stratigraphy of the Bowland Basin. BS Bowland Shale Formation; PG Pendle Grit; PL Pendleside Limestone Formation; HL Hodderense Limestone Formation; PSM Pendleside Sandstone Member; RLM Ravensholme Limestone Member; PLM Park Style Limestone Member. After Earp et al. (1961), Aitkenhead et al. (1992) and Waters et al. (2009). Abbreviated stages are Serpukhovian (Serpukhov.) and Holkerian (Hol.).

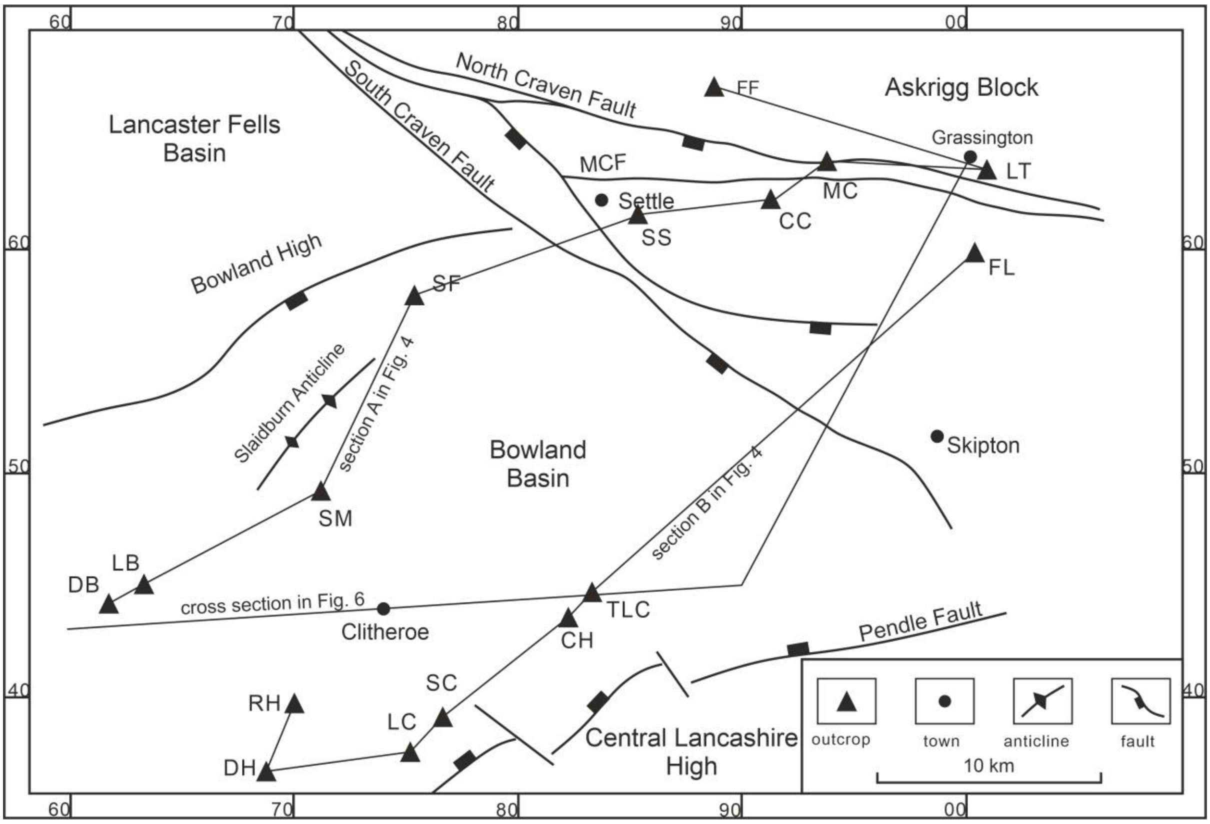

Fig. 2 Study area in the Bowland Basin, Craven Fault Belt (between the South and North Craven Faults), and the southern Askrigg Block and location of study sections (see Table 1). MCF - Mid Craven Fault, CC – Cow Close, CH – Clough Head Beck, DH – Dinckley Hall, SF – Dob Dale Beck, DB – Dobson's Brook, FF – Fountain Fell, FL – Fell Lane, LT – Linton Church, LB – Leagram Brook, LC – Light Clough, MC – Moor Close Gill, RH – River Hodder, SS – School Share, SM – Smelthwaite Farm, SC – Swardean Clough, TLC – Tory Log Clough.

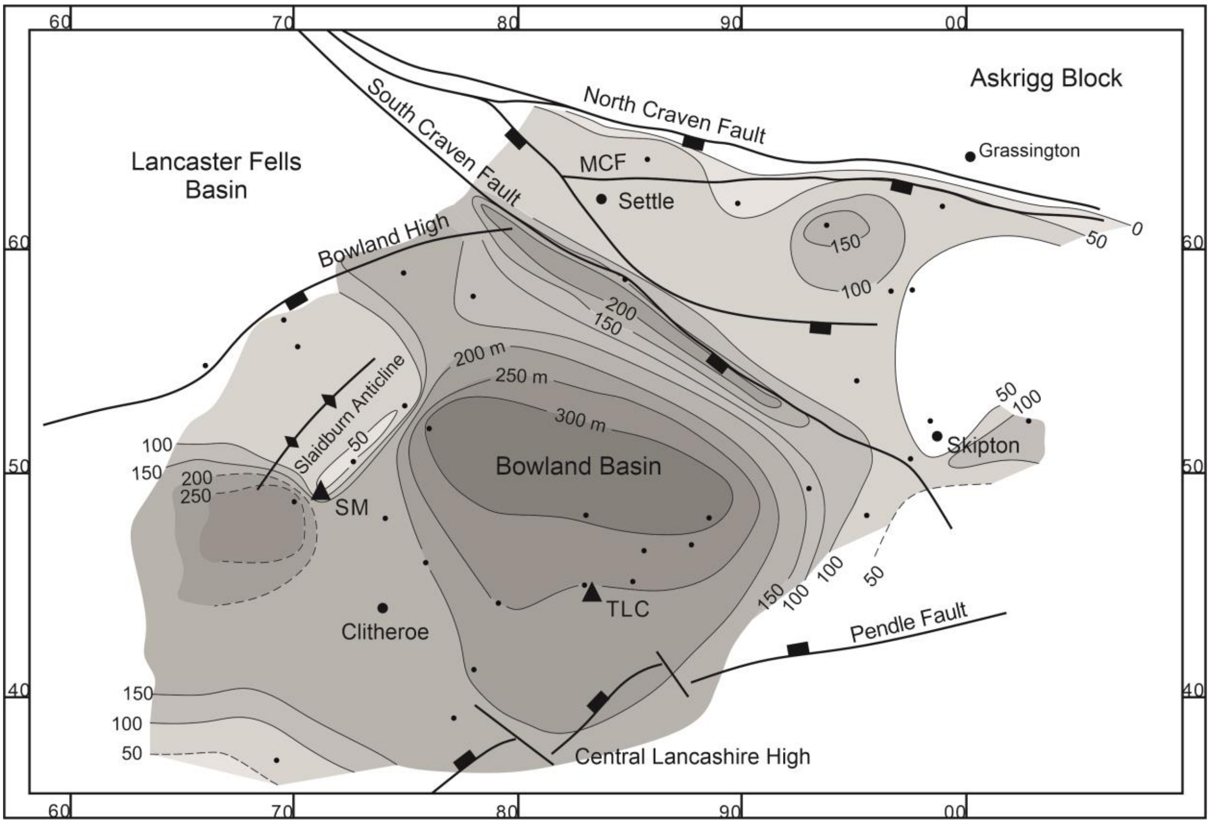

Fig. 3 Isopach map of the Asbian-Brigantain-aged Bowland Shale Formation showing the influence of structural features (Craven faults and the Slaidburn Anticline) on sediment thickness. Dots represent locations of thickness data, primarily derived from the records of Geological Survey memoirs.

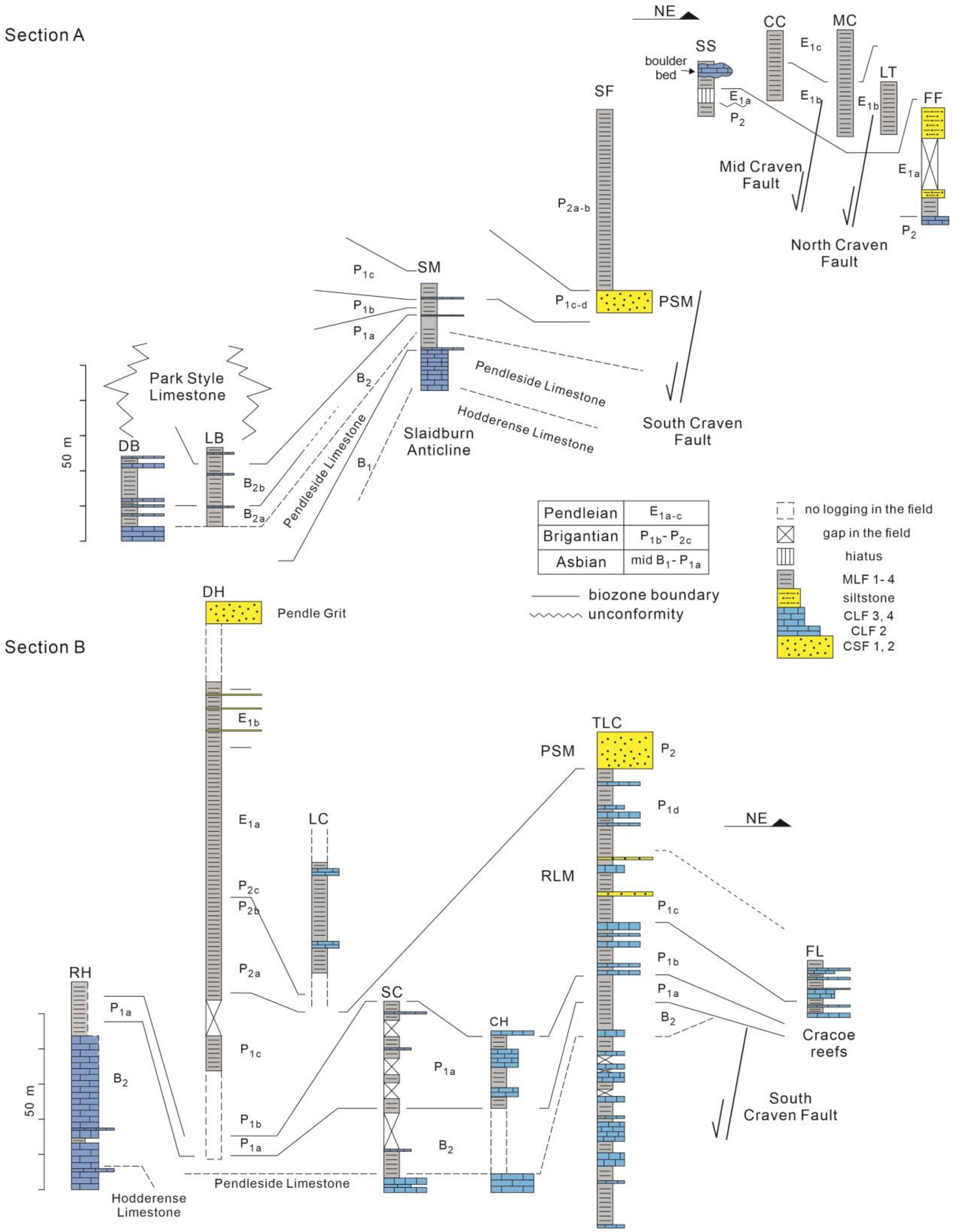

Fig. 4 Correlation panels for Bowland Shale sections along two NE-SW transects from the margins to the centre of the Bowland Basin (see Fig. 2 and Table 1 for outcrop details). RSM Ravensholme Limestone Member; PSM Pendleside Sandstone Member; MLF mudstone lithofacies; CLF carbonate lithofacies; CSF siliciclastic sandstone lithofacies (see lithofacies section in the main text).

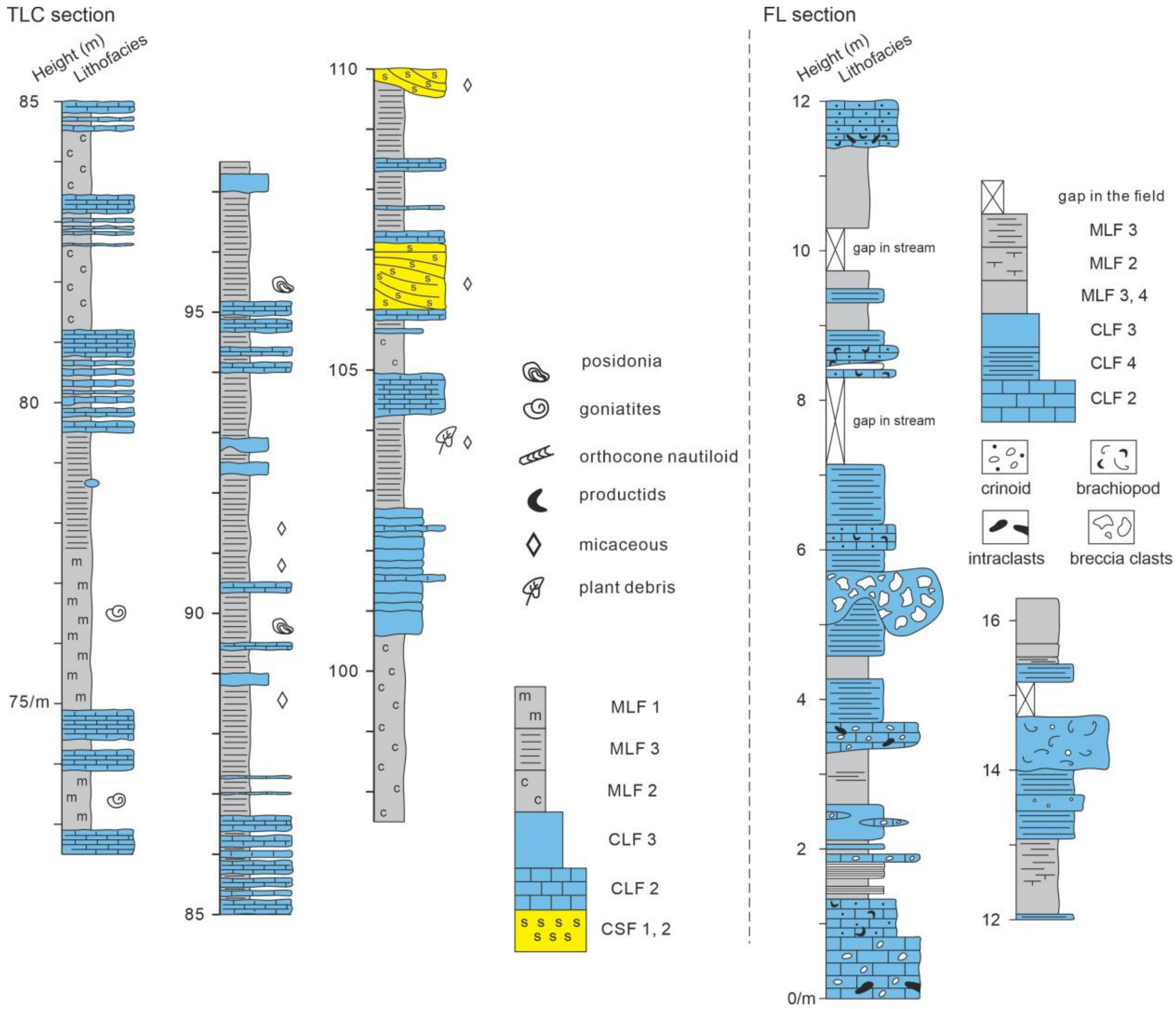

Fig. 5 Sedimentary logs of the lower Bowland Shale showing the diverse range of facies types developed at this level. (A) Basinal Tory Log Clough (TLC) section, ranging in age from the late Asbian – Brigantian (cf. Fig. 4), showing numerous limestone interbeds (this is a typical style of development of the Ravensholme Limestone Member). The strata below 73 m height (not shown) belongs to the underlying Pendleside Limestone Formation; the topmost bed at 110 m height marks the erosive-base base of the Pendleside Sandstone Member. (B) Sedimentary log of the basalmost Bowland Shale developed at the Fell Lane section (basal Brigantain age, cf Fig. 2) showing interbeds of several limestone facies notably boulder-bearing beds (CLF 1) with typical Bowland Shale dark mudstone lithologies. Note that some mudstones MLF 3 and 4 mudstones cannot be distinguished without thin section study.

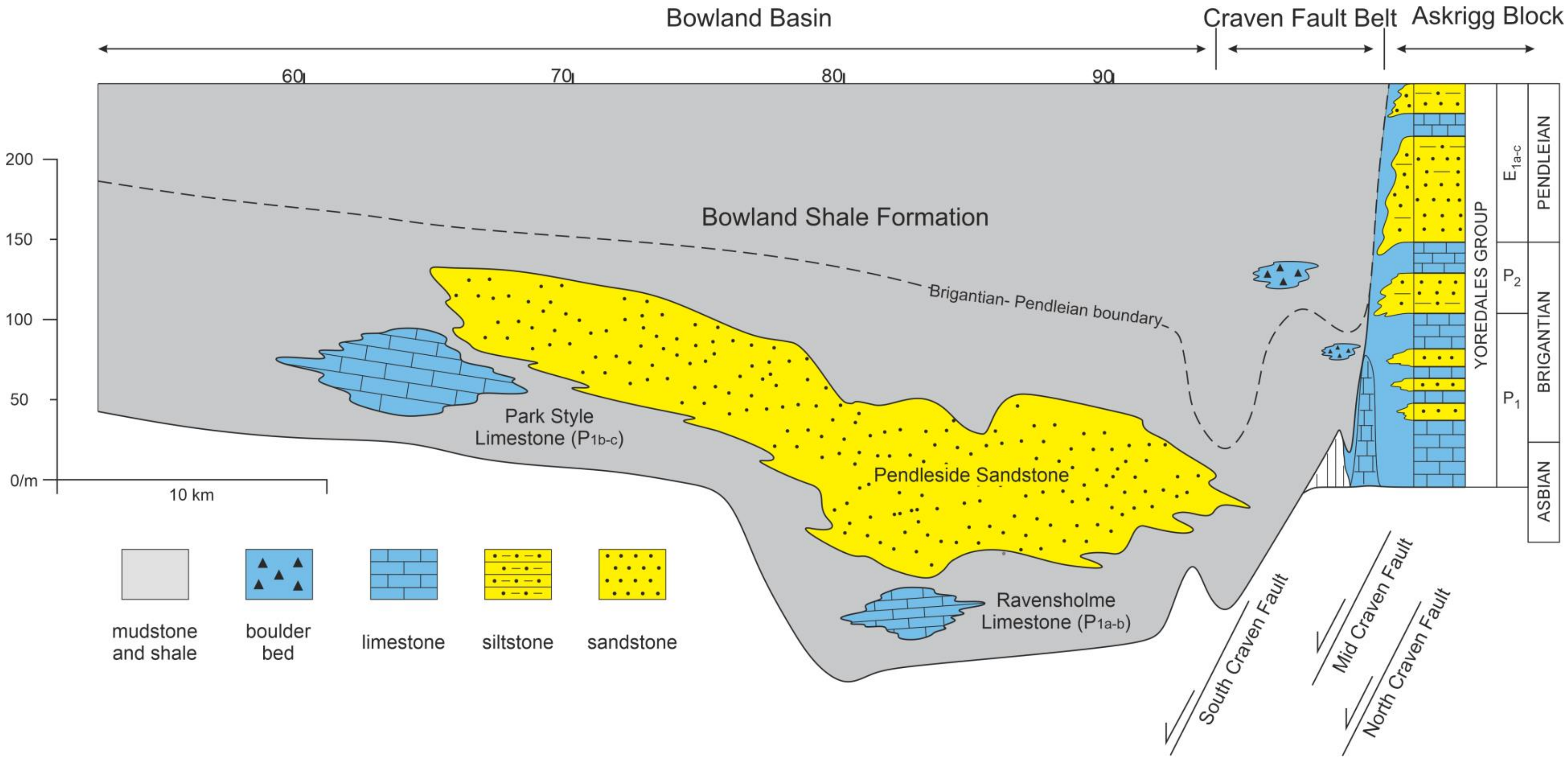

Fig. 6 Cross section from the southern margin of the Askrigg Block to the southern-most outcrops of the Bowland Basin (see line of section in figure 2), showing the thick development of the Pendleside Sandstone in the lower part of the Bowland Shale, and levels of main limestone units and the laterally equivalent lithologies of the Yoredale Group. MLF for Mudstone Lithofacies, CLF is carbonate lithofacies and CSF is clastic sandstone lithofacies.

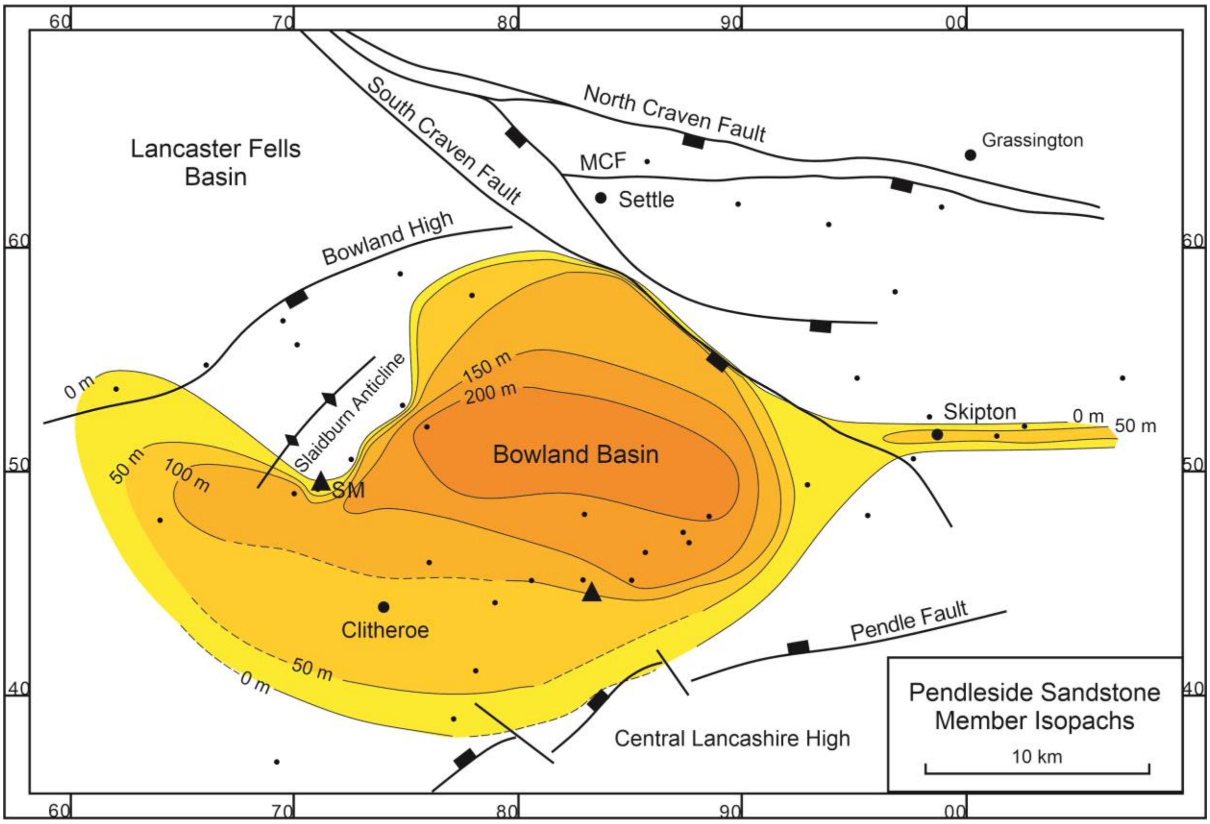

Fig. 7 Thickness variations in Pendleside Sandstone in the Bowland Basin. Isopachs are dashed where data density is low. Sections where thicknesses have been measured denoted with a • and elsewhere thicknesses have been estimated from the maps of the British Geological Survey.

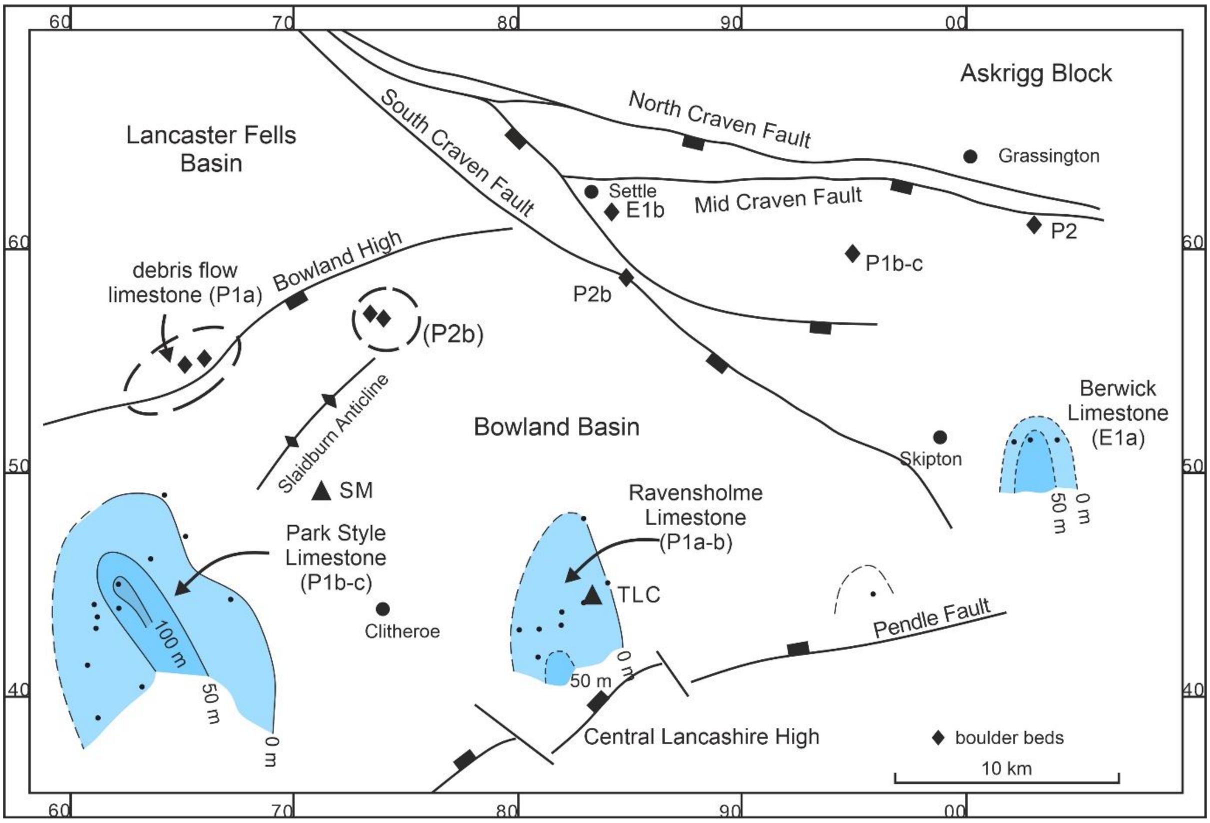

Fig. 8 Isopachs for carbonate bodies developed in the Bowland Shales and location of localised, limestone boulder beds.

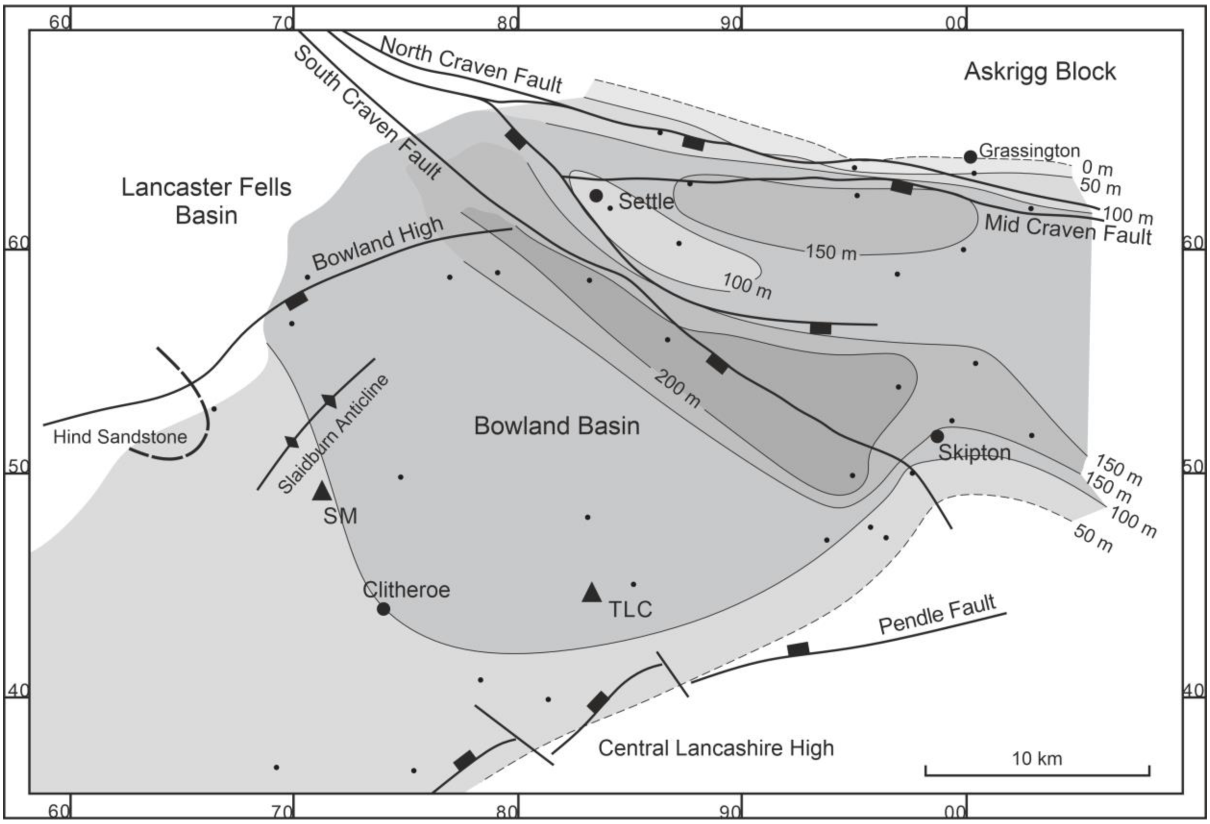

Fig. 9 Isopach map of the Pendleian-aged Bowland Shale Formation in the Bowland Basin and Craven Fault Belt area showing principal depocentres adjacent to bounding faults.

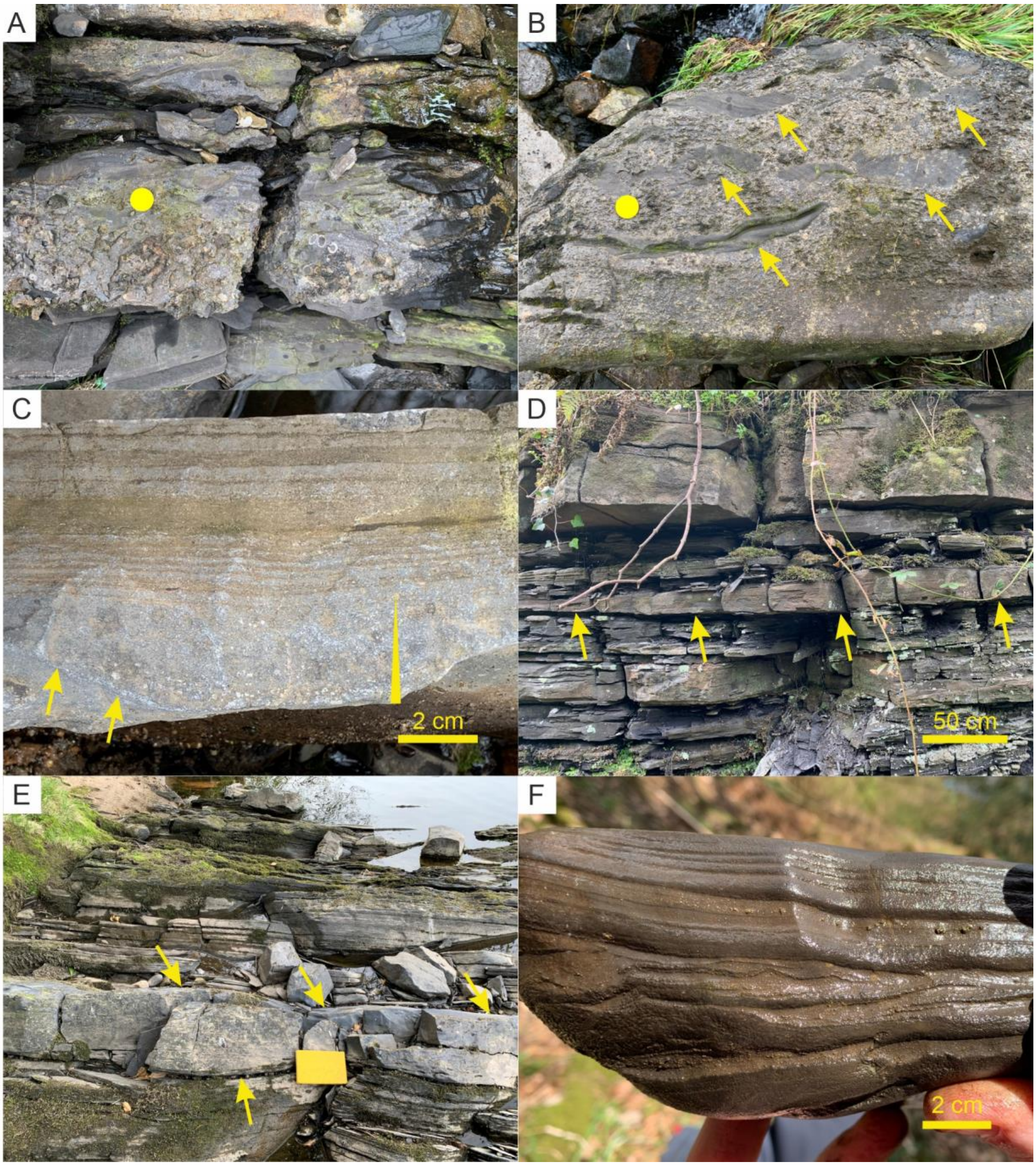

Fig. 10 Field photographs of carbonate beds in the Bowland Shale. (A) Coarse calcirudite bed (CLF 1), dominantly composed of crinoid columnals, P_{1b} subzone, Fell Lane section. The yellow disc is 14 mm in diameter. (B) Coarse calcirudite bed (CLF 1), loose block, showing large tabular clasts of Bowland Shale, P_{1b} subzone, Fell Lane section. Yellow disc is 14 mm in diameter. (C) Loose block of CLF 2 bed showing massive, graded lower part (T_a division) of coarse calcarenite grading upwards into fine-grained, laminated strata (T_b division), B_{2b} subzone, Dobson's Brook section. (D) CLF 2 bed displaying a broad hummock (yellow arrows denote base), whilst overlying (topmost) bed is graded, and nearly 1 m thick, B_{2b} subzone, Dobson's Brook section. (E) limestone bed (CLF 4) displaying hummock-like topography, E_{1b} subzone, Dinckley Hall section. Yellow notebook is 20 cm in length. (F) Block of CLF 2, a hummock-like bedform with laminae showing a simple thickening of beds from right to left. Internally, minor soft sediment deformation or possibly small oscillatory structures are developed, B zones, Dobson's Brook.

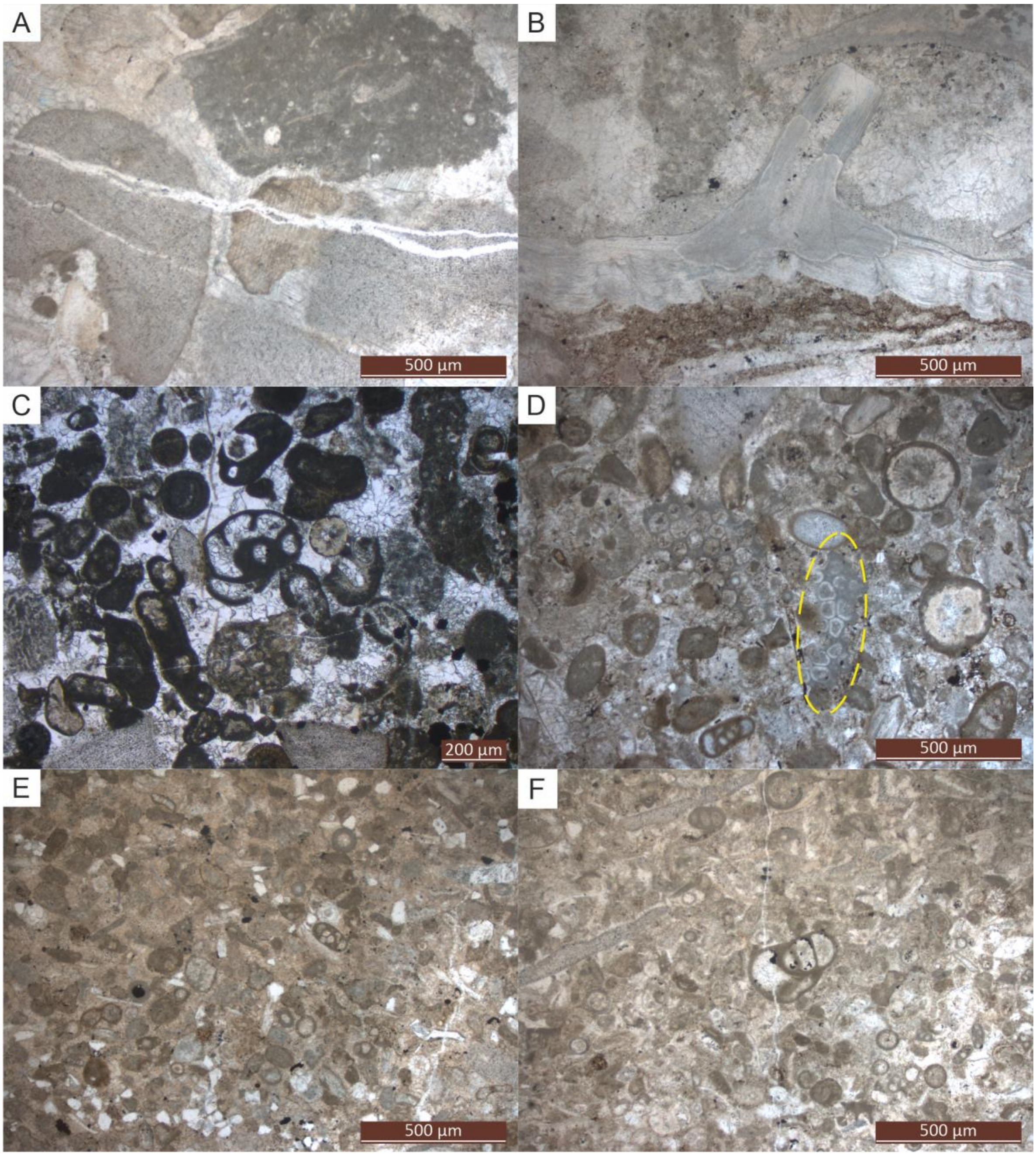

Fig. 11 Thin section photographs of limestone facies from the Bowland Shale. (A) CLF 1 coarse calcirudite with crinoid bioclasts and wackestone intraclast, P_{1b} subzone, Fell Lane section. (B) CLF 1 coarse calcirudite with large brachiopod shell with broken spine attached. The matrix shows a mix of micrite and sparry patches, P_{1b} subzone, Fell Lane section. (C) CLF 2 coarse calcarenite/grainstone dominated by peloids, with foram and crinoid bioclasts, basal P_{1a} subzone, Tory Log Clough section. (D) CLF 2 coarse calcarenite composed of peloids, crinoid columnals (showing micrite envelopes), calcareous algae (*Koninckopora,* outlined) and forams. B_{2a} subzone, basal Lower Bowland Shales, Dobson's Brook. (E) CLF 2 calcarenite dominated by peloids, intraclasts with micrite envelopes and rarer quartz grains, B_2 zone, basal-most Lower Bowland Shale, Swardean Clough. (F) CLF 2 fine calcarenite/ pack-grainstone with peloids, coated grains, forams and possible micritised brachiopod shells, B_2 zone topmost bed of the Pendleside Limestone, immediately below base of Lower Bowland Shale, Swardean Clough.

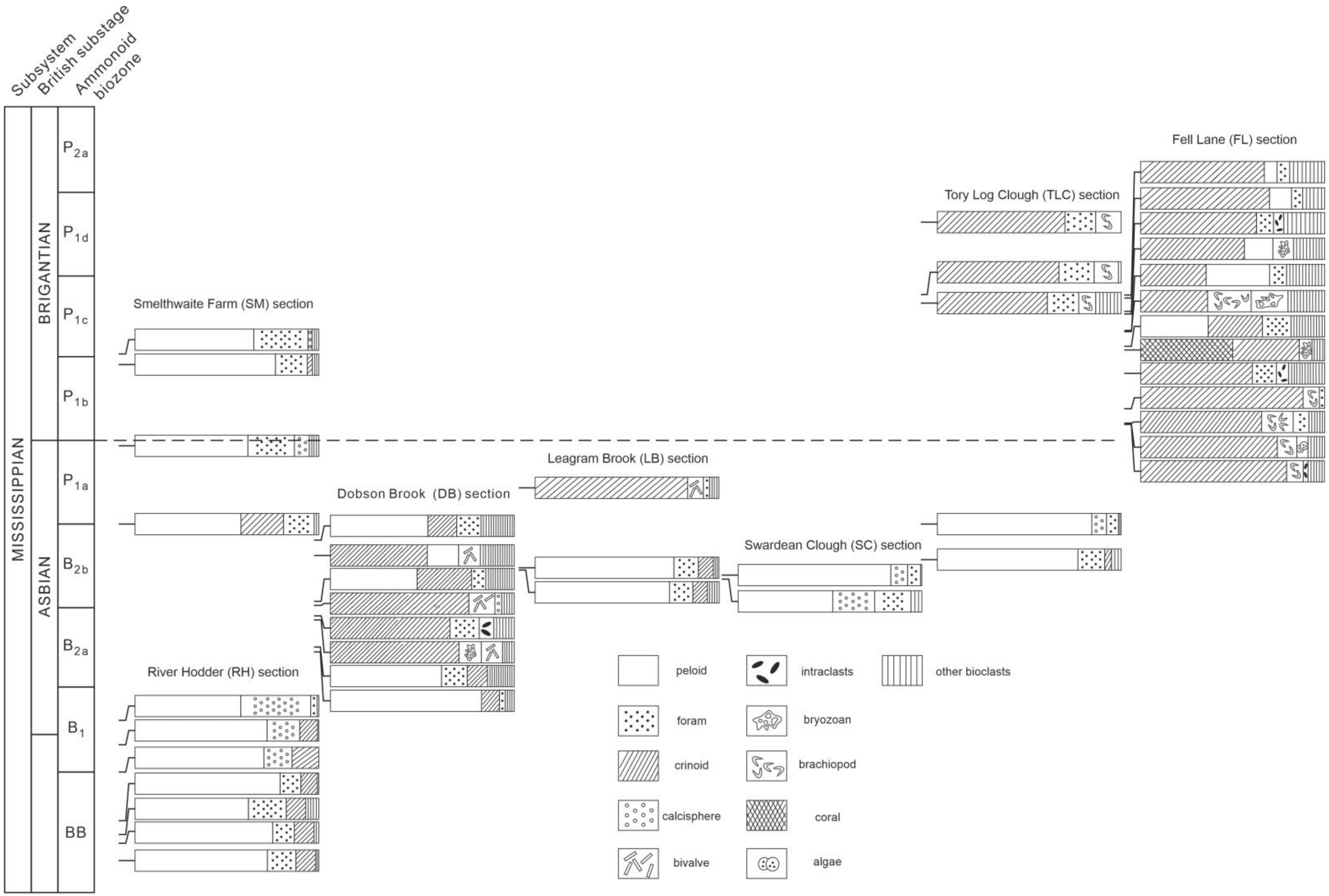

Fig. 12 Evolving composition of allochthonous carbonates (CLF 2) found within the Asbian- Brigantian in the Bowland Basin. River Hodder data are from the Pendleside Limestone, all other data from the Bowland Shale. The three most abundant clast types are displayed whilst others are included as 'other bioclasts'. There is a broad transition within the Basin from peloid-dominated to crinoid dominated carbonates, the exception being the ultra-condensed Smelthwaite farm section where peloidal carbonate dominates throughout.

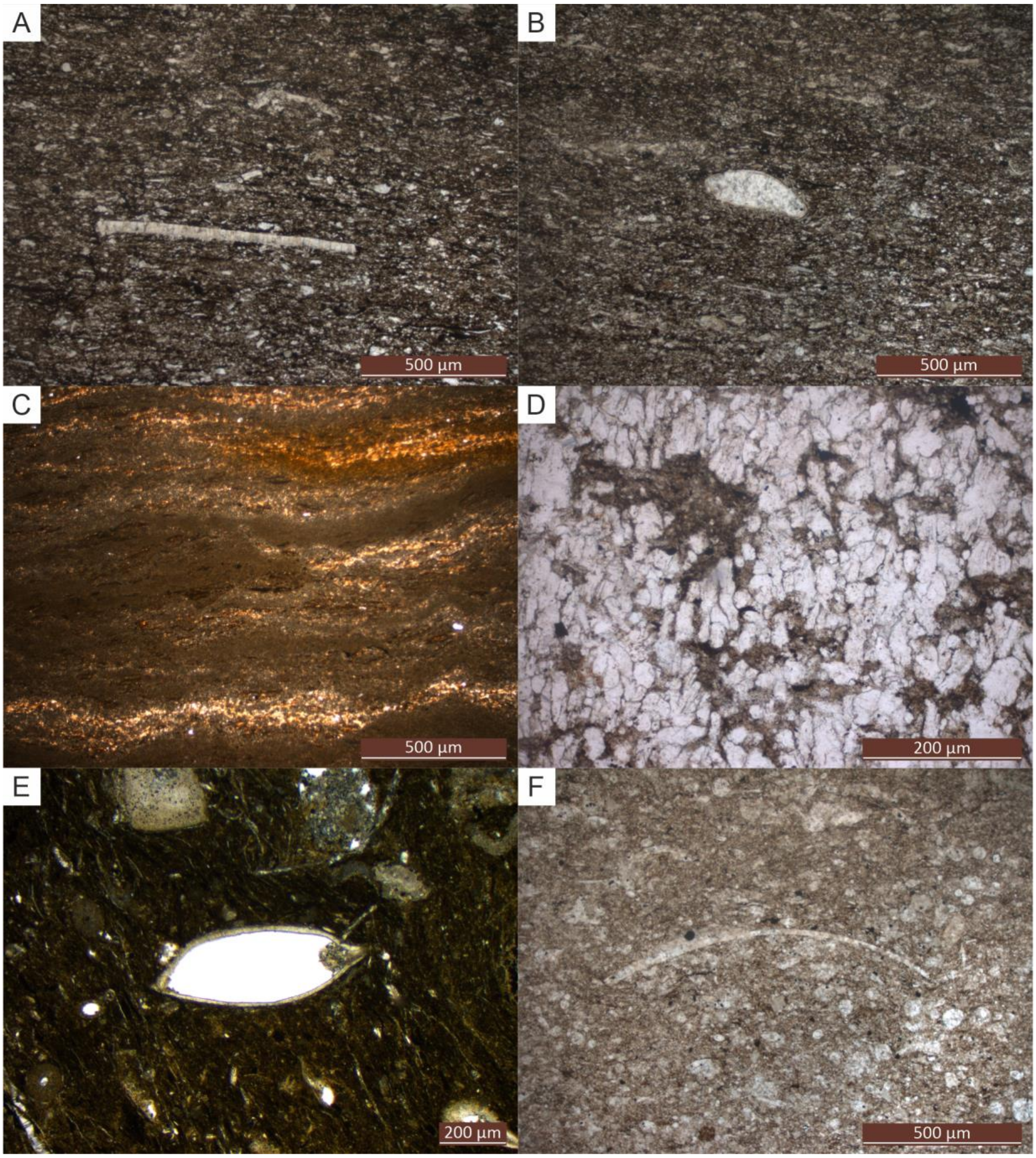

Fig.13 Thin section photographs of limestone facies from the Bowland Shale. (A) CLF 3, calcisiltite with a fragment of mollusk skeletons showing prismatic structure, P_{1b} subzone, Fell Lane, (B) CLF 3 calcisiltite with spar-filled ostracod, P_{1b} subzone, Fell Lane, (C) CLF 4 micritic limestone displaying wavy lamination partially recrystallised to microspar, uppermost E_{1a} subzone, Dinckley Hall, (D) CLF 4 Microspar consisting of laths/stumpy prisms orientated vertically and showing a weak radial or fan-like arrangement, basal P_{1c} subzone, Smelthwaite Farm, (E) CLF 5, ostracod and crinoids in wackestone, basal P1a subzone, Smelthwaite Farm. (F) CLF 3 bioclastic wackestone bearing calcispheres and a thin-shelled bivalve, B_{2b} subzone, Dobson's Brook.

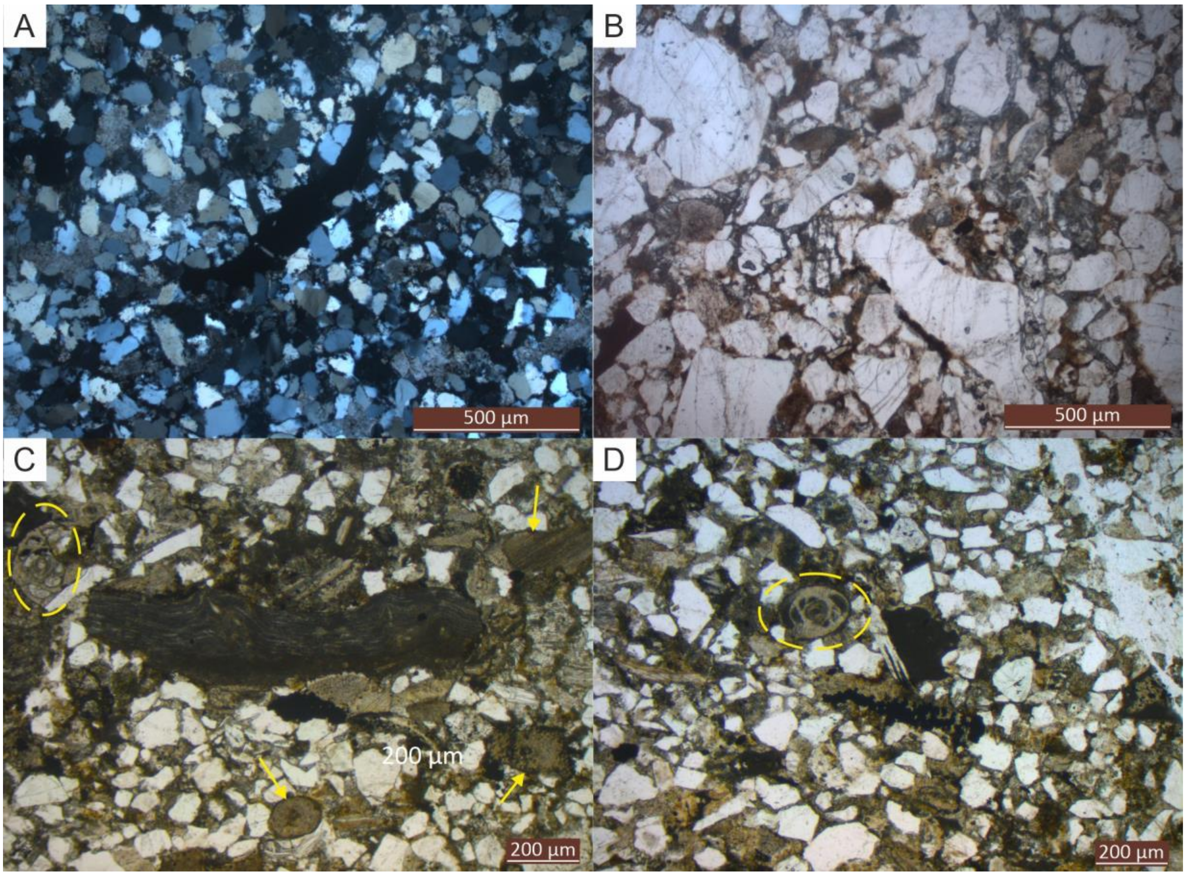

Fig. 14 Thin section photographs of clastic sandstone lithofacies from the Bowland Shale. (A) CSF 1 well sorted, fine sandstone seen in cross-polars, P_{1d} subzone, Tory Log Clough. (B) CSF 1 medium-fine grained sandstone with poor sorting, lower E_{1b} subzone, Dinckley Hall. (C) CSF 2, bioclast-rich sandstone containing brachiopod fragments (central), crinoid fragments (yellow arrows) and a foram (yellow circle, *Archaediscus*), basal P_{1d} subzone, Tory Log Clough. (D) CSF 2, bioclast-rich sandstone with forams (yellow circle, *Archaediscus*), basal P_{1d} subzone, Tory Log Clough.

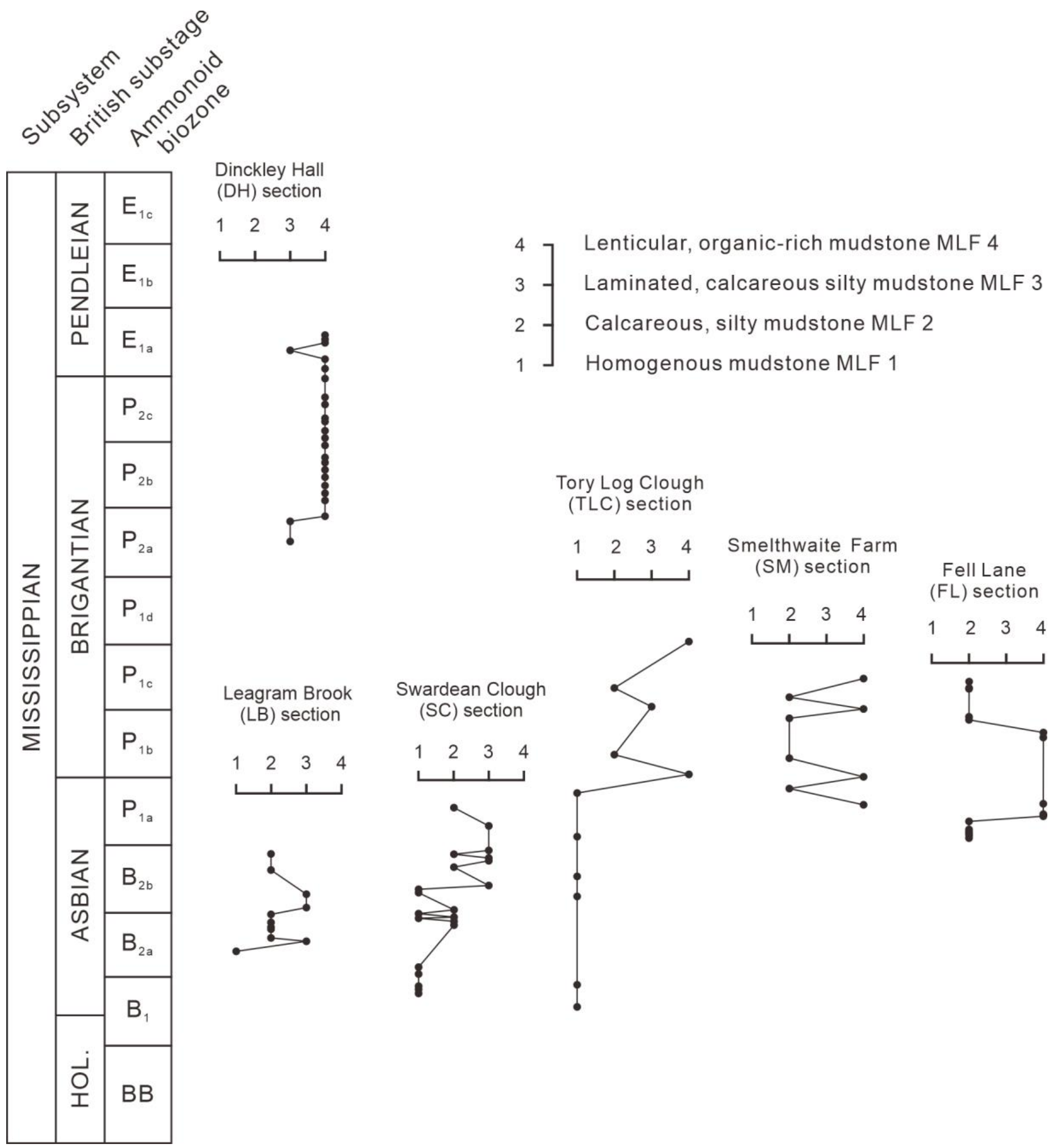

Fig. 15 Stratigraphic variation of mudrock facies in selected Bowland Shale outcrops showing the increasing importance of organic-rich mudstones with abundant clay lenses (MLF 4) in younger strata at the expense of more carbonate-rich mudrock facies. HOL - Holkerian.

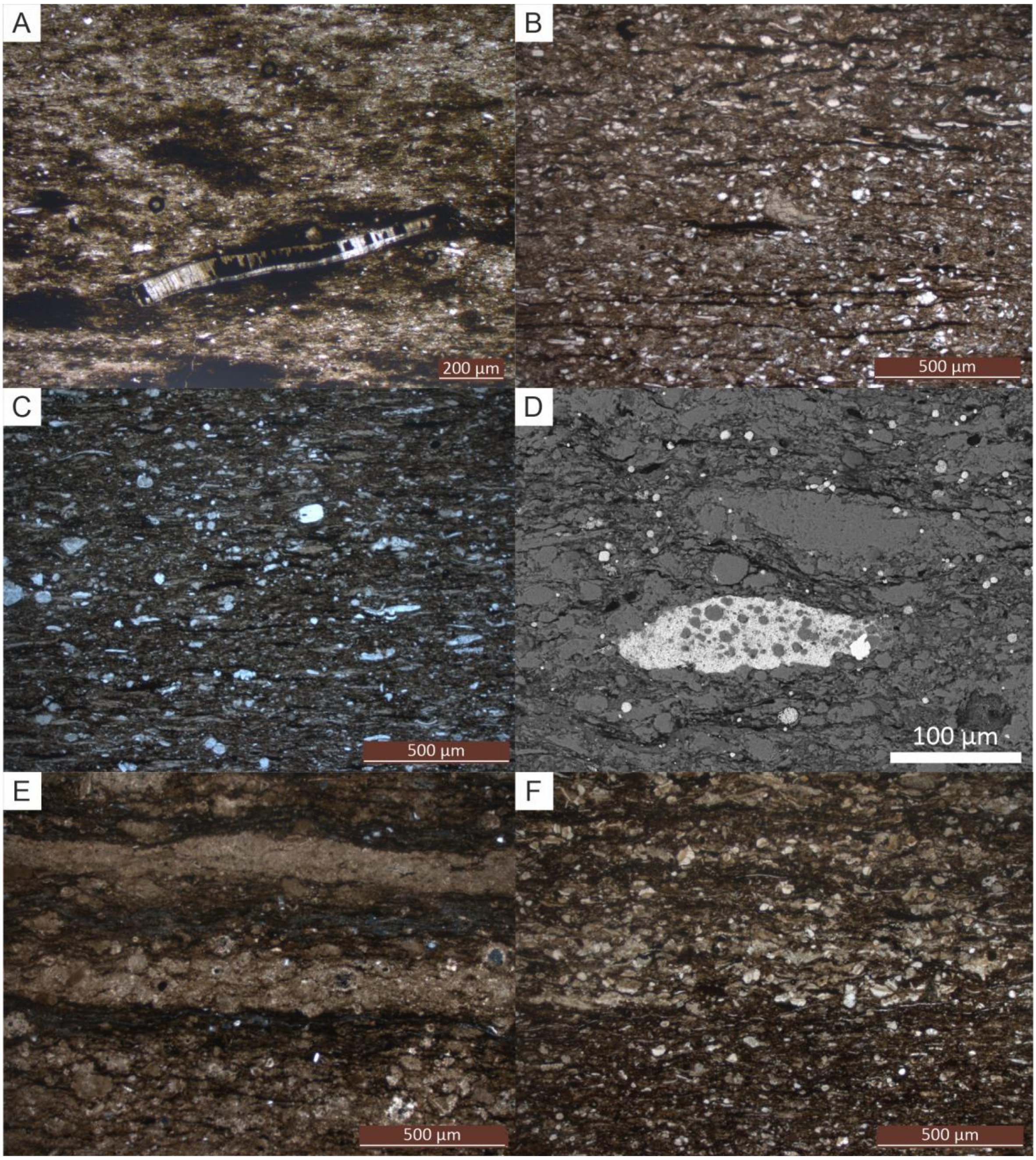

Fig. 16 Thin section and SEM photographs of mudrock facies from the Bowland Basin. (A) MLF 1 homogenous mudstone with mollusk skeletons showing prismatic structure and partial pyritic replacement, B_2 zone, basal lower Bowland Shale, Tory Log Clough. (B) MLF 2 calcareous, silty mudstone with common organic filaments, topmost Pendleside Limestone, B zone, Swardean Clough. (C) MLF 2 calcareous, silty mudstone with common bioclast fragments, B_{2a} subzone, basal lower Bowland Shale, Dobson's Brook. (D) MLF 2 SEM image showing abundant carbonate grains (light grey), clay minerals (dark grey), organic matter (black) and pyrite (bright colour) in the form of small, spherical framboids and a pyrite lens incorporating carbonate clasts, P_{1b}-P_{1c} boundary, Smelthwaite Farm. (E) MLF 3 laminated, calcareous mudstone consisting of carbonate-rich and clay rich laminae, P_{1a} subzone, Swardean Clough. (F) MLF 3 laminated, calcareous mudstone consisting of carbonate-rich laminae composed of angular calcisilt (fragmented bioclasts?) with clay and organic-rich laminae, uppermost P_{1a} subzone, Swardean Clough.

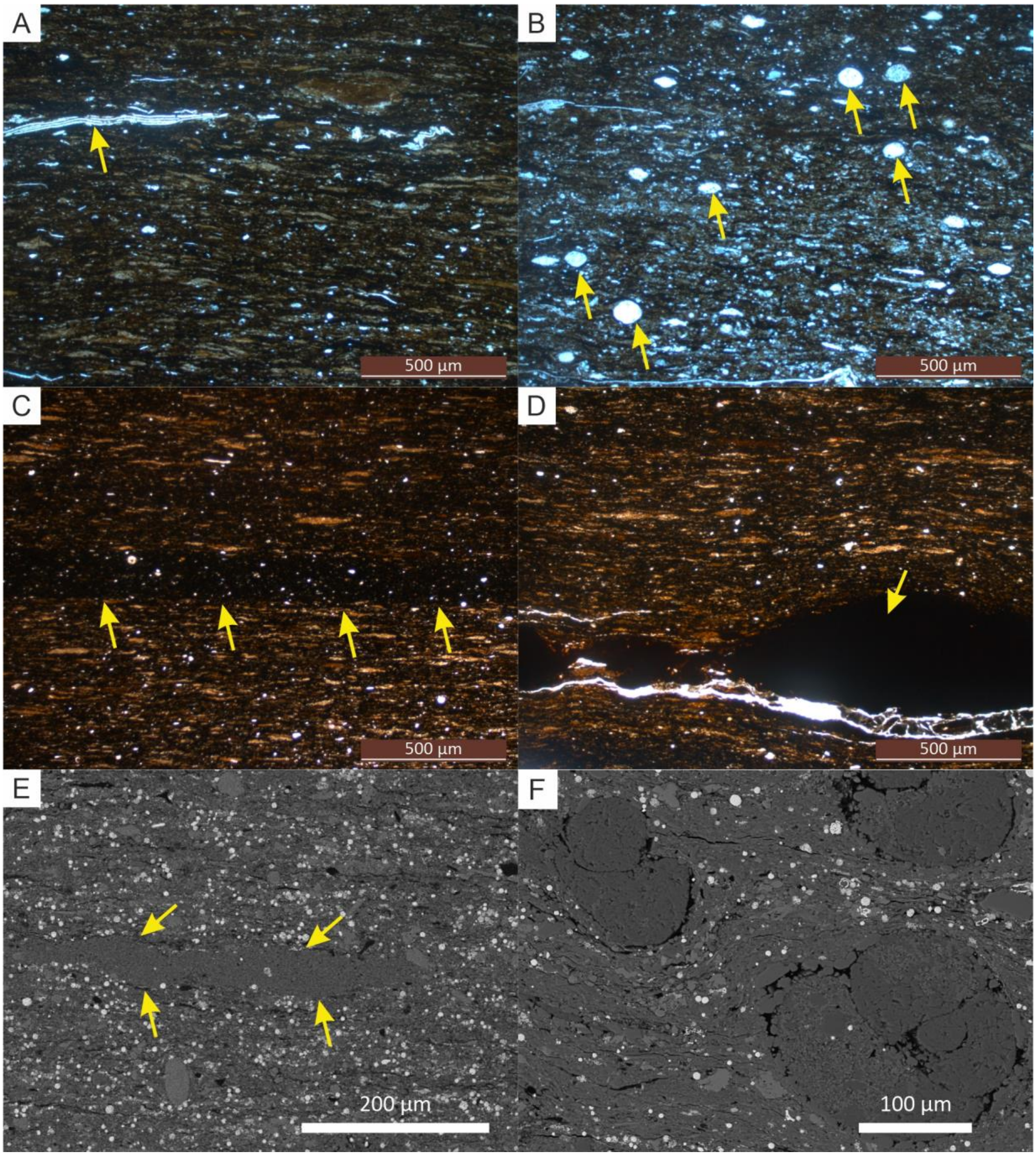

Fig. 17 Thin section and SEM photographs of lenticular, organic-rich mudrocks, MLF 4, from Dinckley Hall. (A) Example showing thin, articulated bivalve prodissoconch (yellow arrow), basal E_{1a} subzone. (B) Example with scattered radiolarians (arrowed), P_{2b} subzone. (C) Example showing typical clay lens-rich layer fabric and a homogenous lamina consisting of clay and organic matter (arrows denote the base), mid E_{1a} subzone. (D) Example with phosphatic nodules (largest example arrowed), mid E_{1a} subzone. (E) SEM image showing a clay lens lacking framboids (delineated by arrows) in a matrix with abundant small framboids (bright spots), lower E_{1a} subzone. The lens is highly mechanically compacted and squeezed, which indicate the primary particle was soft, ductile, and water-rich. (F) Example with several ammonitellas (larval goniatites) in a matrix rich in framboids and clay lenses, basal P_{1c} subzone.

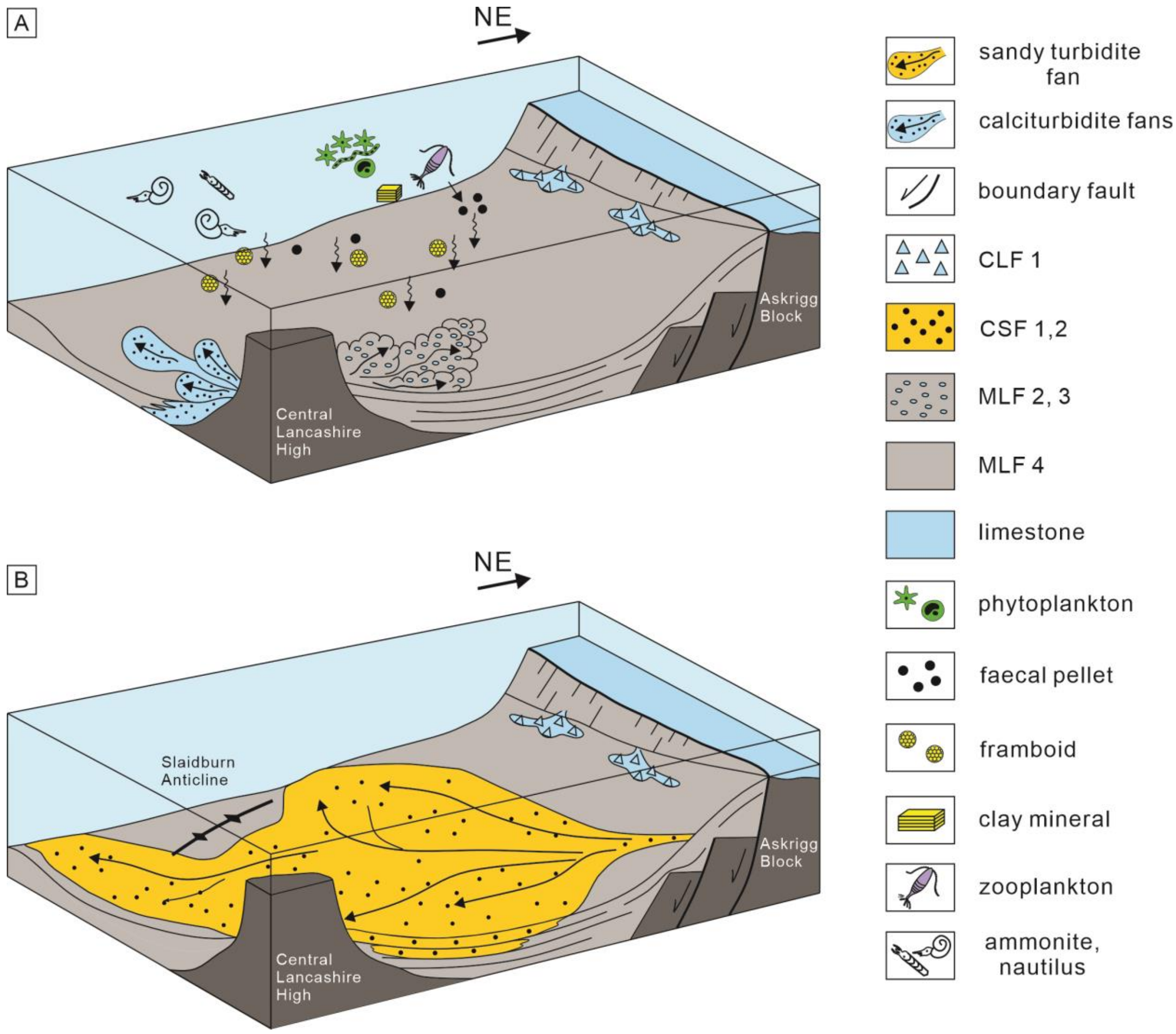

Fig. 18 Schematic models for the deposition of the Bowland Shale in the Bowland basin. (A) illustrating the diverse deposition processes of different lithofacies mentioned in the text, showing a combination of pelagic and hemipelagic settling and shedding of carbonate detritus, especially from the Central Lancashire High. (B) depositional model for the Pendleside Sandstone, sourced from a narrow channel in the NE of the basin with the down-dip development showing deflection around the intrabasinal high formed by the Slaidburn Anticline.